The geology and tectonics of central Bhutan

The Geology and Tectonics of central Bhutan

Lucy V. Greenwood[1], Tom W. Argles[1]*, Randall R. Parrish[2,3], Nigel B.W. Harris[1], Clare Warren[1]

[1] The Open University, Walton Hall, Milton Keynes, MK7 6AA

[2] University of Leicester, University Road, Leicester, LE1 7RH

[3] NERC Isotope Geosciences Laboratory, British Geological Survey, Keyworth

*Corresponding author (email: tom.argles@open.ac.uk)

Number of words of abstract (216), text (9832), references (2295) and figures (12) = 12343 words plus figures

Abbreviated title: Tectonic architecture of the eastern Himalaya

Abstract

Lithotectonic mapping, metamorphic observations and U-Pb zircon ages underpin a substantial revision of central Bhutan geology – notably a more extensive and continuous outcrop of the Tethyan Sedimentary Series (TSS) than previously mapped. Metamorphic grade in the TSS increases downward towards a basal north-vergent tectonic contact with the underlying Greater Himalayan Series (GHS), interpreted as a southward continuation of the South Tibetan Detachment (STD). Miocene (~17 – 20 Ma) leucogranite sheets are associated with the STD in this region but appear to diminish southwards. Two leucogranite dykes that cross-cut TSS structures yield ages of 17.8±0.2 and 17.9±0.5 Ma. A 500±4 Ma (U-Pb zircon) metamorphosed ash bed in the Pele La Group within the psammite-dominated lower TSS yields the first direct isotopic age for the TSS in the eastern Himalaya, confirming existing age constraints from detrital zircon and fossil studies. A continuation of the Paro metasedimentary unit underlying the GHS was mapped near Wangdue Phodrang. Our observations, notably the exposure of a wholly ductile STD so far south and the significance of large nappe-like structures in the TSS, prompt a major revision to the geological map of the Bhutan Himalaya and require a reassessment of tectonic interpretations of the Bhutan Himalaya.

Keywords: Himalayan Geology, Bhutan, South Tibetan Detachment, Tethyan Sedimentary series, Leucogranite, Geochronology

Supplementary material: Zircon U–Pb geochronological data, sample locations and descriptions, features of analysed zircons, sample processing methodology and detailed analytical conditions are available at http://www.geolsoc.org.uk/SUP18876

Geological Background

The eastern Himalaya is the least understood major segment of the mountain belt. Despite the tectonic template of major units and bounding faults available in the rest of the Himalaya (Figure 1), there remain fundamental disputes about the identity and correlation of stratigraphic packages, the nature and location of the major contacts between those units, and the timing of orogenic processes in the region. Resolving these unknowns is particularly critical in the light of recent suggestions that the eastern Himalaya differs from the central and western portions either in component materials, tectonic architecture, orogenic mechanisms, or all of the above (e.g. Yin *et al.* 2010a, b; Webb *et al.* 2013).

The broad-scale geology along much of the Himalayan arc including Bhutan (Figure 1) is remarkably uniform. At the highest structural level is the Tethyan Sedimentary Series (TSS), a deformed, mainly low-grade package of sedimentary rocks deposited on the Indian margin of the Tethyan Ocean from Neoproterozoic to Mesozoic times. The basal TSS, which may reach amphibolite grade in places (Chambers *et al.* 2009; Tangri & Pande, 1995; Schneider & Masch 1993; Yin 2006), overlies high-grade metasedimentary gneisses of the mainly Neoproterozoic Greater Himalaya Series (GHS) on a generally low-angle, north-directed normal fault system, the South Tibetan Detachment (STD; Burchfiel *et al.* 1992). The GHS in turn overlies generally low-grade Palaeoproterozoic to Permian sedimentary rocks of the Lesser Himalayan Series (LHS) on a major south-directed thrust, the Main Central Thrust (MCT; Heim & Gansser 1939). A distinctive feature of the Himalayan core is evidence for Miocene exhumation of the GHS by broadly synchronous displacement on the STD and MCT, resulting in the significant contrast in grade across the two contacts (Burchfiel & Royden 1985; Hodges *et al.* 1992; Grujic *et al.* 1996; Grasemann *et al.* 1999; Chambers *et al.* 2011), and the generation of peraluminous leucogranites that were typically emplaced just below or along the STD (Griesbach 1891; Le Fort *et al.* 1987; Harris & Massey 1994).

We present a geological map of Bhutan in Figure 2, redrawn to incorporate our new data, and also a comparison of some previous geological maps of Bhutan, in simplified form, to show how interpretations of the outcrop configuration have evolved (Figure 3). Despite early geological investigations in Bhutan by Godwin-Austen (1868), Mallet (1875), Pilgrim (1906) and Hayden (1907), it was not until the work of the Indian Geological Survey and Augusto Gansser (1964 & 1983) that much of the country was explored and mapped. Gansser's (1983) map has proved a firm foundation for all recent studies of the geology of Bhutan, the principal inaccuracies occurring from relationships extrapolated in the absence of *in situ* observations. More comprehensive coverage was achieved by the lesser-known work of the Indian Geological Survey, compiled by Bhargava (1995). More recent studies

(Swapp & Hollister 1991; Wu *et al.* 1998; Grujic *et al.* 2002, 2011; Yin 2006; Kellett *et al.* 2009; Long & McQuarrie 2010; Tobgay *et al.* 2010; Long *et al.* 2011a; Chambers *et al.* 2011; McQuarrie *et al.* 2013) have sought to resolve the inconsistencies within and between these maps.

Problems addressed in this study

Both Figures 2 and 3 highlight some major features of Bhutan's geology that are unique in the mountain belt and demand investigation:

1) Major differences amongst previous work with regards to the interpretation of the map pattern and the extent of rocks assigned to the GHS and TSS; an objective of this paper is to address this topic.

2) Extensive outcrops of the TSS, previously mapped as isolated klippen south of the primary trace of the STD along the main orogenic watershed in northern Bhutan/southern Tibet (e.g. Gansser 1983). These outcrops include some of the most southerly exposures in the mountain belt of the TSS, which crops out ~8 km from the MCT in southern Bhutan south of Zhemgang, and nearly as closely in eastern Bhutan (this study; Bhargava 1995; Grujic *et al.* 2002). Our work helps clarify this map pattern.

3) The gently to moderately dipping structurally conformable contact of the TSS klippen that separates the lower psammite-dominated TSS Chekha and other formations from upper amphibolite facies GHS rocks beneath. This contact has generally been mapped as a southward continuation of the STD, though it preserves only ductile shear fabrics in contrast to the northern STD, which exhibits both ductile and brittle deformation (Edwards & Harrison 1997; Wu *et al.* 1998; Grujic *et al.* 2002; Kellett *et al.* 2009). However, recently some authors have proposed that the GHS and TSS comprise a stratigraphically continuous section in southern Bhutan, mapping this contact as a stratigraphic transition rather than a tectonic break (Long & McQuarrie 2010) and calling into question criteria used to discriminate between basal TSS (Chekha Formation) and upper GHS lithologies.

4) The upper carbonate-dominated TSS is more prevalent to the north and closer to the STD than the psammite-dominated TSS, which is thick and extensive adjacent to the STD in more southerly outcrops (see Figure 2). There has to be either a stratigraphic or structural reason for this observation; we provide an explanation.

5) The significantly thickened GHS section in Bhutan (e.g. Daniel *et al.* 2003), consisting of two GHS 'panels' separated by an amphibolite facies sequence of probable TSS rocks. This configuration is considered to be due to southerly displacement on the out-of-sequence Kakhtang Thrust (KT) from ~16 – 10 Ma (Davidson *et al.* 1997; Gansser 1983; Grujic *et al.* 2002; Warren *et al.* 2011). This thrust has

been traced intermittently from eastern Bhutan through to the Trongsa region, but its continuation further westward has not been mapped – if indeed it persists at all. At present no direct analogue of the Kakhtang thrust has been reported in Sikkim or further west in the Himalaya, though it may continue into Arunachal Pradesh as the "Zimithang Thrust" (Yin *et al.* 2006). Previous studies have plotted mostly speculative courses for the KT into western Bhutan: turning south of the Gophu La granite and either passing north of the northern termination of the Tang Chu klippe and Punakha (Grujic *et al.* 2002) or tracking further north towards Gaza in NW Bhutan (Long & McQuarrie, 2010); turning north of the Gophu La granite and connecting with the ductile Laya Thrust in NW Bhutan (LT; Figure 2; Grujic *et al.* 2011), which like the KT is characterised by the southward emplacement of an uppermost amphibolite to granulite facies sequence of gneisses over an amphibolite-bearing unit (Warren *et al.* 2011). We address the possible north-western extent of the KT in this study and its relationship with the Gophu leucogranite.

6) The occurrence of a structural window of mainly middle amphibolite-grade metasedimentary rocks of the Paro metasediments of Gansser (1983), as an eastward extension to the major structural dome south of Paro in western Bhutan. These rocks lie structurally beneath upper amphibolite facies rocks of the GHS and may correlate structurally with a thin sliver of schists known as the Jaishidanda Formation (Jangpangi 1974; Gansser 1983; Ray *et al.* 1989; Dasgupta 1995; McQuarrie *et al.* 2013).

7) A pattern of younger N-S and E-W broad folds that exert a major control over the map pattern of Bhutan. This study discusses the age of these folds relative to each other and to the MCT and Main Boundary Thrust (MBT).

Methods

Geological mapping and petrography

The detailed geology was mapped during expeditions in 2008, 2009 and 2010 via transects, either along roads or trekking paths (Figure 2). GPS coordinates for localities mentioned in text or shown in figures are in the Supplementary file. Some mapping of lithology, contacts and/or structural trends was possible by observation of better-exposed areas adjacent to transect routes. Samples (locations in Figure 2) and structural measurements were taken *in situ*, with some remote observations using Google Earth imagery. Where structural orientations of planar and linear features are shown on maps, our data are either representative of numerous measurements within a certain area (tens of metre to a few kilometre scale) or are measurements that represent a large area on the basis of orientation of geological contacts. Petrography was used to supplement geological data, assess metamorphic state of

rocks, and provide insight into the relationship between mineral growth and fabrics associated with various macroscopic structures; we present numerous pelite mineralogical and petrographic descriptions in the Supplementary file as well, though in this we have relied upon observations of other studies for quantitative metamorphic P-T assessment where relevant.

Structural analysis comprised a broad field-oriented approach, making field observations of primary features (e.g. fossils, cross-bedding, conglomeratic layers, bedding), early axial plane cleavage and layer-parallel micaceous foliation, folded and crenulated foliations, features indicating simple shear and/or flattening (mineral lineation of various grades, boudinage, c-s fabrics, rotational features, pebble flattening), relationships of mica and other porphyroblasts to fabric elements, and in some areas geological mapping of major lithological boundaries to define folds and repetition of units.

Criteria for assignment of rocks to geological units: basis for map revision

Major differences in large scale outcrop patterns of the GHS, TSS and Paro metasediments exist on published maps of Bhutan (Figure 3). Differences between our map and that of Gansser (1983) mainly arise from revisions in areas not visited by Gansser and from re-interpretation of the affinity of medium-grade metamorphic rocks. More significant are differences between our results and those of Long, Tobgay, McQuarrie and co-workers in various contributions including their geological map of Bhutan (Long *et al.* 2011). We have also been guided by observations of Bhargava (1995) in a little-cited publication that covered a significant area of central Bhutan. Our criteria for assigning rocks to TSS, GHS, or Paro metasediments follow the framework accepted by researchers across the Himalaya and documented well by Gansser (1983); nevertheless we reiterate those important criteria here (Table 1) in the interests of clarity.

The lowermost Tethyan Sedimentary Series. All workers recognise within the TSS a higher stratigraphic upper carbonate-dominated portion above a psammite-dominated portion with variable amounts of phyllitic to fine-grained schist at lower amphibolite grade. The latter comprises the Chekha Formation of Gansser (1983, also referred to as Sangsing La formation); it is regarded as either early Palaeozoic (presence of Palaeozoic detrital zircons – Long and McQuarrie, 2010) or latest Neoproterozoic (Bhargava 1995) in age. We place this formation firmly within the TSS, based on its psammitic lithology and moderate metamorphic grade. This lowest part of the TSS invariably lies upon the GHS. Using these criteria, significant areas of rocks assigned to the GHS by Long and McQuarrie (2010) and Long *et al.* (2011) are reassigned here to the TSS.

Discrete shear zones: criteria for identification

Major high-strain shear zones are key features of the Himalaya and have been mapped by numerous workers using similar criteria to ours (Table 2): intensity and gradients of shear strain, juxtaposition of different lithologies and significant gradients in metamorphic grade. We use these visible criteria to map discontinuities between the highly strained, high-grade GHS and either the strongly folded and cleaved TSS or the deformed LHS. While brittle overprints may be present, ductile fabrics are predominant. In fact the STD in central Bhutan is wholly ductile, appearing less dramatic than the brittle-ductile STD exposed along the crest of the Himalaya to the north as described by Burg *et al.* (1984) and Burchfiel *et al.* (1992), but displaying the same top-to-north shear sense.

U-Pb geochronology

Samples for zircon U-Pb geochronology were collected from one ash bed and three granitic rocks in central and southern Bhutan (see Figure 2 for locations). Zircons were extracted from rock samples by crushing and milling followed by separation with a Rogers© table, heavy liquids and a Frantz© magnetic separator. Methods are detailed further below and in the supplementary material.

LA-ICP-MS analysis

Zircons were analysed using laser ablation multi-collector inductively-coupled plasma mass spectrometry (LA-MC-ICP-MS) at the NERC Isotope Geosciences Laboratory (NIGL), Keyworth, UK. Small (<100 µm long), elongate, inclusion-free crystals were hand-picked under a binocular microscope, avoiding grains with optically-visible cores. One group of grains were mounted in an epoxy disk, polished and imaged using cathodoluminescence scanning electron microscopy (SEMCL), on a FEI QUANTA 600 ESEM with a tungsten tetrode electron gun and a Centaurus CL detector, at 10nA, 15mm working distance at the British Geological Survey, UK to investigate zoning patterns and to choose appropriate spots for analysis. A second group of zircons were mounted in epoxy but left unpolished. Laser ablation for U-Pb isotope analyses was performed at NIGL using a UP193FX (193nm) excimer or UP193SS (193nm) Nd:YAG system (New Wave Research, UK), coupled to either a Nu Plasma HR multi-collector or a Nu AttoM magnetic sector single collector inductively-coupled mass spectrometer (ICP-MS). Instrumental configuration and measurement procedures followed methods described in Thomas *et al.* (2010, 2013). Reference zircons (GJ-1, Plešovice, 91500) were used resulting in a U-Pb calibration uncertainty of ~2.5% 2σ, which was quadradically added to final age results.

Laser spot analysis (with typical spot sizes of 10 – 20 μm) was undertaken on the polished grains, the location of laser spots being guided by the CL images. However, because overgrowth rims were typically narrower than the laser spot size, an external surface rim rastering technique (Cottle *et al.* 2009) was employed on unpolished zircon grains. The aim was to obtain age data exclusively from the thin rims of grains, within a few microns of the top surface, thereby avoiding inherited cores. Time –series evaluation of the data was, however, used to determine whether any older zone was penetrated.

ID-TIMS analysis

Zircons from the ash bed sample (LG-09-21) were analysed using chemical annealing isotope dilution thermal ionisation mass spectrometer (CA-ID-TIMS) methodologies at the NERC Isotope Geoscience Laboratory (NIGL). Prior to dissolution zircons were subject to a modified chemical abrasion pre-treatment designed to eliminate Pb-loss (Mattinson, 2005). The accuracy of the presented $^{238}U/^{206}Pb$ dates is controlled by the gravimetric calibration of the EARTHTIME U-Pb tracer (ET535) employed in this study and the determination of the ^{238}U decay constant and isotopic composition of uranium (Jaffey *et al.* 1971; Condon *et al.* 2007). Uncertainties on Pb/U ratios are typically 0.1%. More information on both methods of geochronology are given in the supplementary files.

Results

Geological mapping of structural relationships

Our observations result in major changes to the map pattern of central Bhutan relative to all previous work. We also clarify structural relationships between geological units, we describe major internal structures within TSS rocks that have not been recognised previously, and we elaborate on the late upright large scale folds that control the geological map of Bhutan.

The extent of TSS in Bhutan

Using the criteria described above, we reassign to the TSS significant areas in southern Bhutan of medium-grade psammitic rocks originally mapped as Paro metasediments or Chekha Formation (lowest TSS) by Gansser (1983) and Bhargava (1995). These same rocks were mapped by Long and McQuarrie (2010) and Long *et al.* (2011) as upper GHS (their unit GHlmu or GHlm), but we are confident that the rocks shown as TSS between Dagana-Damphu and Wangdue Phodrang, and the westward-narrowing synclinal keel of TSS above the GHS between longitudes 89.5°-90.3°E, are entirely analogous with the psammite-dominated TSS rocks between Sure and Trongsa (Figure 2). We also document the STD shear

zone separating the GHS (footwall) and TSS (hanging wall) in southern Bhutan, consistent with metamorphic and lithological observations of Gansser (1983), Long and McQuarrie (2010), and Corrie *et al.* (2012).

Farther north, we show as a continuous unit the TSS in the Black Mountain and Tang Chu areas, consistent with the work of Bhargava (1995), and extend this large area of TSS to the east side of the Gophu La granite, on the basis of new mapping.

Early structures within the TSS

Our mapping near the southern margin of the Gophu La granite (Figure 2) extends the TSS outcrop significantly. In the Thampe Chu valley a sequence of south-dipping TSS strata clearly overlies the Gophu La leucogranite, and appears to be right way up (Figure 4a, b), similar to the sequence proposed in the Tang Chu klippe by Tangri & Pande (1995) and greatly resembling a section east of Punakha (Gansser, 1983, Fig. 54, p.55). The sequence is: intrusive and sheared leucogranite at the base; a thin band of psammite and phyllite intruded by veins of leucogranite next (unit TSSq on Figure 5); laminated impure limestone with narrow bands of psammite and pelite overlain by massive, cliff-forming pure limestone (unit TSSl on Figure 5), and brown slates and phyllites (unit TSSp on Figure 5) at the top. Note the absence of a significant thick quartzite typical of the lower TSS (Chekha Fm.) farther south (e.g. near Pele La) which would be expected stratigraphically to crop out between the GHS/Gophu La granite and the carbonate-dominated upper units.

The rocks are mainly low to medium greenschist facies, reaching low amphibolite facies just at the base and in some areas more widely. The basal contact with the Gophu La leucogranite has a strong flattening and shear fabric and is relatively planar, despite the presence of leucogranite bodies that range from nearly massive to foliated. Evidence for top to the north shear was observed as uncommon S-C fabrics, but also conjugate deformed (shortened/extended) pre-existing veins of thin leucogranites. This sequence unambiguously refutes interpretations that the Gophu La leucogranite structurally *overlies* the TSS rocks (e.g. Long *et al.*, 2011) and is consistent with Gansser's (1983) observation of leucogranite beneath TSS in the bottom of the upper Tang Chu valley near its headwaters, southwest of our mapping. This sequence was also mapped on the west side of the Nikha Chu valley (Figure 5) and to the east-northeast of Thampetso La (Figure 4a,b; 5), but the same strata appear to be inverted in the eastern Nikha Chu side valley east of locality LG-10-22 (Figure 4d). The map-scale probable inverted stratigraphy, bedding dips and gently dipping cleavage in the area of Figure 5 is most simply explained by the presence of large scale (500 m), tight to isoclinal, overturned folds that can be interpreted as

verging to the north-west within the TSS as shown in the map and cross section in Figure 5. We specifically infer a northward-opening synform with the TSSp pelitic unit in its core.

Further evidence for relatively large-scale folding in the TSS lies in folded bedding on outcrop scale within TSS sediments (Figure 4 c-f). The widespread cleavage in moderately competent rocks and penetrative foliation within more micaceous lithologies associated with these folds appears to be the earliest structural foliation within the TSS rocks. These folds were observed in the majority of limestone outcrops and to a lesser extent in psammite and finer grained clastic rocks, both in the Nikha Chu area and throughout TSS outcrops in central Bhutan. The majority are nearly recumbent, tight to isoclinal folds with broadly east-west or SW-NE trends. Most metre-scale folds of this type observed in the Nikha Chu area appear to verge to the north in terms of their asymmetry. These characteristics suggest that small-scale folds are associated with large-scale overturned folds like those mapped in the Nikha Chu area. Farther south and east from the axial traces of these overturned/recumbent folds (southern portion of Figure 5), the strata dip north and west, exposing an analogous, sheet-like leucogranite body beneath the TSS rocks, with GHS gneisses underlying it. The GHS rocks here are continuous with those exposed in a later, larger, gently west-plunging open antiform of GHS gneiss (that can be traced much further east into the Trongsa-Bumthang area as shown in Figure 2). This major structure post-dates the juxtaposition of the TSS with the GHS and controls the map pattern of a large area of central Bhutan. This antiform was inferred and mapped by Gansser (1983) and Long *et al.* (2011), respectively.

Alternating cleavage-bedding relationships were measured at ~15 roadcuts between localities 21 and 43 (Trongsa–Sure road) through the large expanse of Chekha and other Tethyan sediments in central Bhutan, and mapped along the well-exposed Zhemgang-Sure transect. Along this transect, cleavage mainly dips less than 30° despite warping by later, large-scale open folds, while bedding may be sub-horizontal or much steeper, indicating that there are folds in bedding but less variable cleavage orientation. Vergence reversals inferred by cleavage-bedding relationships indicate the presence of multiple near-recumbent fold hinges at various scales, implying that folding is widespread in the TSS but seldom exposed well-enough to be mapped in this densely forested area, in contrast to the Nikha Chu area. The predominant orientation of the cleavage relative to bedding generally has bedding dipping more steeply within hinge regions with cleavage at a low angle; other than in hinge regions, the bedding – cleavage relationship is best interpreted as indicating asymmetric folds with an apparent vergence southwards (apparently upright limb longer than overturned limb), consistent with south-directed shear in this area by Long and McQuarrie (2010). We appreciate the apparent difference in vergence of large scale folds relative to the northern region, but feel it is important data with general consistency over this distance of ~ 20km; we comment later on its significance. Surprisingly, large-scale

fold structures in the TSS of Bhutan have not previously been described and are likely to have been extensively overlooked. The widespread occurrence of tight-isoclinal mesoscale folds with gently-dipping axial planes implies much larger-scale folds with a similar attitude. TSS units of central Bhutan are likely deformed into several large fold-nappes, similar to those in the external zones of the European Alps (Lugeon, 1902; Termier, 1904; Heim, 1921), and to north-verging structures mapped in the TSS rocks above the STD in the Annapurna region of Nepal (Gansser 1964; Godin *et al.* 1999).

Figure 6b presents a schematic sketch of this structure, which shows how contrasting apparent thicknesses of units in different locations can be reconciled with the overall structure. In the Pele La area, a thickened package of psammite-dominated rocks stratigraphically underlies the upper thick carbonate unit and overlies the GHS. By contrast, to the north at Thampe Chu the psammitic rocks have been sheared and thinned, while the overlying carbonate package appears thickened by folding and its base is very close to the STD, in contrast to further south. The general observation in central Bhutan that quartzites dominate TSS sections in the south whereas carbonate lithologies dominate in the north is clear from the mapping of Gansser (1983), Bhargava (1995) and our study, and is shown in Figure 2. We suggest that in general, this pattern can be explained by their relative positions in this major fold nappe and by the later attenuation of units due to shearing along the basal structural contact with the GHS, as implied in Figure 6b. Another possible explanation is that the psammite-dominated unit was originally much thicker in the south, thinning rapidly to the north where stratigraphically overlying carbonate units are thicker. Although possible, we have no basis of assessing this and given the structural complexity, we assert that a structural explanation is more plausible.

Figure 6b also shows a possible configuration of the thicker and more widespread Gophu La granite and its southward continuation into a thinner sheet-like unit intruding into the underlying GHS gneisses, as implied by our mapping further south. We suggest as one possibility that the attenuation of lower TSS units is a later, separate feature related to the STD, but leave open the extent to which these two events – large north-verging recumbent folding and STD motion – were separated in time. We address some timing constraints of these events below.

TSS (klippen) – basal contacts

In many locations the contact between the GHS and the overlying TSS is obscured by peraluminous Miocene leucogranite intrusions, which appear to have been emplaced in the uppermost GHS; many are 10-100 m thick, too small for their outcrops to be shown on the maps in this paper. Veins or dykes of leucogranite were observed intruding the overlying lower TSS rocks at several locations (e.g. Figure 7a) as well as GHS rocks in some cases (e.g. north-east of locality LG-10-14, Figure 5a). Three cross-

cutting leucogranites have been dated (two in the TSS, one in the GHS; see Geochronology section). The leucogranites commonly take the form of sills in the south, with larger bodies (on a 10-50 km scale) in the north, including the Gophu La granite shown in Figures 4-5; where observed, their relationship with the TSS rocks is broadly sill-like and concordant (though demonstrably intrusive on outcrop scale). A few leucogranites are foliated, exhibiting planar fabrics parallel to the foliation in the country rock, and in some cases inter-fingering with GHS gneisses (Figure 7b). Most leucogranites are relatively unfoliated at outcrop scale, but are certainly folded later, along with their host stratigraphic units, into broad synclines and anticlines. The observation that leucogranites are found primarily near the structural contact between the GHS and TSS suggests (but does not prove) that they were emplaced during part of the displacement along this shear zone, after the main nappes were formed (Figure 7a), perhaps due to decompression in the footwall of this structure.

Where the basal contact of the TSS klippe is exposed with no substantial intervening leucogranite, such as at locality 43 or as described by Chambers *et al.* (2011), it is a ductile shear zone up to ~300m thick juxtaposing sillimanite-grade paragneiss or orthogneiss of the underlying GHS with garnet-staurolite schist overlain by foliated to more massive buff quartzite of the Chekha Formation with cross-stratification sporadically visible. The contact zone is defined by high shear strain relative to the rocks above and below and associated with shear sense indicators that are predominately top-to-the-north (Figure 8a-c). In this zone, the shear fabrics deform an earlier foliation in both footwall and hanging wall, though the earlier fabrics in each should not be correlated. By contrast, the dominant shear sense observed in the GHS gneisses is top-to-the-south (Figure 8d-f), which is much more prevalent at lower structural levels within the GHS and especially dominant near the MCT.

The TSS-GHS contact was investigated on three main transects: the Trongsa-Gelephu road, the Wangdue-Damphu road, and the Thimphu-Phuentsoling road (Figure 2). Our observations are similar to several other descriptions of the STD in Bhutan (Chambers *et al.* 2011; Grujic *et al.*, 1996, 2011; Kellet *et al.*, 2010).

Trongsa-Gelephu transect

At locality LG-09-9 near Trongsa, pale thinly-bedded quartzite interbedded with fine-grained, flaggy pelitic schists may represent the basal Chekha Formation of the TSS that overlies high grade gneiss and migmatite of the GHS which are intruded by leucogranite. Banded calcareous amphibolite and a fine grained amphibole-biotite-plagioclase layer here may represent metavolcanic units (perhaps of the Singhi formation; Tangri and Pande, 1995). The pelitic schists contain muscovite, biotite, mainly syn-kinematic garnet and randomly-oriented late or post-kinematic staurolite, implying that staurolite

growth outlasted the deformation that formed the foliation. Foliation in schist is strong, and where layering is folded we also observe a folded earlier fabric, but the actual contact is partly obscured by intervening leucogranite. We infer a shear zone here as part of the STD as also inferred by Long and McQuarrie (2010), though kinematic indicators are not well-developed. Further south from LG-09-9, within schist and thin psammite, the strike of foliation trends more south-easterly in a broad curve or bend, before trending more southerly near locality LG-09-21, where quartzite is dominant with little schist. Psammite dominates between localities 21 and ~43 and includes some coarse conglomerate layers.

Two kilometres north of locality LG-09-43 (north of Sure), coarse-layered, foliated or weakly foliated buff-coloured Chekha quartzite overlie ~ 100-200m of garnet-staurolite schist that in turn overlies strongly foliated GHS orthogneiss just south of locality 43. The garnet-staurolite schist lacks any sign of migmatisation, and hence is considered to mark the base of the TSS; schists display reasonably abundant top-to-the-north shear sense indicators including S-C fabrics, shear bands, extended and boudinaged veins in favourable orientations and asymmetric detached isoclinal folds, (Figure 8). The sequence of rocks at locality 43 that contains this shear zone is ~ 200-300m thick structurally, with most asymmetric shear sense indicators in a zone ~50m thick; they are better developed in the garnet-staurolite schist than in orthogneiss of the uppermost GHS.

Wangdue-Damphu transect

A section of the TSS is exposed for ~20 km along this road section (Figure 2), composed of thickly-bedded white-buff quartzites and micaceous psammites, thin fine-grained garnetiferous pelites and rare, banded layers with epidote, plagioclase and amphibole, which are likely to have been tuffs. These tuffs may be part of the Singhi volcanics which lie at the base of the Pele La formation within the TSS. Although at upper greenschist and possibly lowest amphibolite grade, the sedimentary character of these rocks is prominent as is the complete lack of high grade minerals or any evidence of partial melting. North and south of this expanse of TSS, outcrops of banded feldspar-quartz-biotite orthogneiss and paragneiss with boudinaged veins represent the GHS. We interpret the TSS outcrop as a westward extension of the Black Mountain TSS massif in a large-scale synform (Figure 2), based on the E-W structural grain of TSS rocks from Zhemgang to Chukha, and opposing dips of GHS rocks at the northern and southern ends of the transect.

In the south the actual contact between the GHS and TSS is obscured by landslide material. The northern basal contact of the klippe was not observed as it is obscured by a vast leucogranite body mapped by Bhargava (1995) that intruded both GHS and TSS. At locality LG-09-77 homogeneous

leucogranite was observed intruded into micaceous TSS quartzite; elsewhere leucogranite intruded TSS mica schists. GHS augen gneiss is exposed structurally below the leucogranite body ~20 km south of Wangdue, just south-east of location LG-09-80 (Figure 2).

At each of these GHS-TSS contacts we infer an important shear zone, on the basis of observations of well-exposed rocks along this zone north of Sure at locality 43 and analogous characteristics of the TSS and GHS rocks near the (unexposed) other contacts.

Thimphu-Phuentsoling transect

The TSS-GHS contact was also investigated at Chukha on the Thimphu-Phuentsoling road, bordering a <5 km wide, east-west-trending outcrop of TSS rocks: low grade quartzite with ~2 cm pelitic layers, limestone and calc-schist. TSS pelites contain garnet, muscovite and much less biotite than in the underlying GHS paragneiss; they also lack any evidence of partial melting or high grade of metamorphism. They are similar in metamorphism and lithologies to TSS rocks already described. The TSS metasedimentary rocks at Chukha form a synformal keel plunging gently to the east (Figure 9, Gansser, 1983). We infer that this TSS outcrop widens to the east (as shown by Gansser, 1983), connecting with the main Black Mountain TSS mapped on the Wangdue-Damphu transect by us and Bhargava (1995). West of Chukha the extent of the TSS synform is unknown but it is likely limited by the easterly plunge of the synform.

The northern contact of the TSS near Chukha separates cliffs of TSS phyllite and quartzite (LG-10-85) from structurally-lower, high-strain GHS kyanite garnet biotite paragneiss (LG-10-84). The contact is not exposed but is inferred to strike east-west and dip moderately south, based on observations and mapping of Gansser (1983).

The southern contact juxtaposes folded, steeply dipping TSS quartzite with mylonitic GHS garnet-mica schist and paragneiss near locality LG-10-94. The contact itself is near-vertical and strikes approximately east-west. We infer that the structural contact is folded here in a tighter 'keel' than that present farther east towards Black Mountain.

Paro window

The outcrop extent of Paro Metasediments in central Bhutan has been revised from Gansser (1983) following mapping along new logging tracks and trekking routes in the areas around Semtokha and Wangdue Phodrang (Figure 10). Two transects near Semtokha pinpointed the Paro-GHS boundary as a contrast between foliated quartzite with phyllite bands (Paro Metasediments) and strongly foliated GHS gneisses (both paragneiss and orthogneiss). The boundary is most easily mapped on the basis of

metamorphic grade and lithological contrast because there is no obvious zone of locally higher strain at the contact.

The main highway east of Thimphu progresses to higher elevations along a sequence of mainly gently east-dipping rocks towards Dochu La, going structurally upwards. Rocks along the road are an east-dipping continuous exposure of biotite and garnet-bearing Paro metasedimentary rocks (garnet-biotite-muscovite schist and semi-pelite) with rare kyanite. Sillimanite-bearing and in part, migmatitic and pegmatite-bearing GHS rocks become common toward Dochu La at structurally higher levels. This section comprises a thick shear zone with strongly foliated rocks throughout, with a transition very similar to that described and illustrated by Gansser (1983, Fig. 71, p,72) north of Paro.

Following from the initial description of Gansser (1983, p.75-76) Paro metasediments were mapped to the north and west of Wangdue Phodrang (Figure 10), comprising a series of muscovite stable pelitic schists, marble bands, quartzite and calc schists, devoid of migmatite. This sequence largely dips gently to the east similar to the west side of Dochu La. Surrounding and structurally above the window is garnet-sillimanite-biotite-K-feldspar (muscovite absent) paragneiss and orthogneiss, characteristic of the GHS. The two metamorphic grades are juxtaposed with the boundary rocks being very strongly foliated, interpreted as a major shear zone. This inlier of Paro metasediments is the eastward continuation of the main Paro window (Gansser, 1983, p. 75-76), but topographically lower on the east side of Dochu La where the antiform plunges eastward beneath the GHS.

Large-scale upright open folds

Our map revision in central Bhutan reinforces a pattern of mainly ~E-W trending upright domes and basins across Bhutan (Figure 2) that control the overall map pattern. The largest of these E-W structures is the synclinal fold from Chukha towards Zhemgang, the extensions to the east of which are the Ura and Radi klippen (Figure 2).

These structures appear to have been deformed by later ~N-S upright folds that cause the E-W structures to plunge east or west. The largest of these N-S structures is the prominent anticline that folds the MCT in the Kuru Chu valley near Mongar and Lhuentse, but the synclinal structure through Black Mountain to the west of Tang Chu is also significant; the GHS rocks dip beneath it on both sides near Wangdue Phodrang on the west, and near Trongsa on the east.

These E-W and later N-S structures both have 50-100 km wavelengths and both post-date the MCT and the juxtaposition of the TSS and GHS (axial traces as shown on Figure 2) along the STD. Because the

Main Boundary Thrust (MBT) in the far south of Bhutan (Figure 2) does not appear affected by any of the N-S folds, it would appear that these two sets of upright folds pre-date the MBT.

A new map of Bhutan

The culmination of structural observations and new mapping in this study is the revised map of Bhutan shown in Figure 2, which is a synthesis of previous mapping, a re-interpretation of some aspects of published work, and our new data and interpolation where no mapping exists. For instance, although we have not been able to access the core of the Black Mountain area, we infer that most of the upland area is underlain by Tethyan metasedimentary rocks: from local structures and from existing mapping of Bhargava (1995) and known Cambrian rocks (Hughes *et al.*, 2011). Similarly, we infer that the TSS metasedimentary rocks observed striking eastwards from the Thampe Chu are connected to very similar lithologies mapped by Gansser to the north and northwest of Bumthang in the footwall of the Kakhtang Thrust, though we have not verified that connection directly. Furthermore, if the Kahktang Thrust continues northwest of Bhumtang it must pass to the north of the TSS metasedimentary rocks mapped in Thamphe Chu and to the north of the Gophu La leucogranite, as shown in Figure 2. Along with our observations presented above, the main sources of data for this new map are Gansser (1983); Bhargava (1995); Grujic *et al.* (2002, 2011); McQuarrie *et al.* (2008); Long and McQuarrie (2010); Long *et al.* (2011a, b); Tobgay *et al.* (2010); Chakungal *et al.* (2010); Edwards *et al.* (1999); Wu *et al.* (1998); Warren *et al.* (2011); Hollister & Grujic (2006); Kellett *et al.* (2009); Daniel *et al.* (2003); Davidson *et al.* (1997); Grujic *et al.* (1996); Kellett *et al.* (2010); Chambers *et al.* (2011); Swapp and Hollister (1991); Richards *et al.* (2006). The principal conclusions arising from the new data and map are:

- A single, folded mass of TSS material in central Bhutan extends more than 150km from a thin synclinal keel in the southwest at Chukha to north-central Bhutan east of Bumthang. This TSS outcrop should no longer be regarded as a series of isolated klippen; in fact arguably this main body of TSS rocks is not even a klippe *sensu stricto* because it is rooted beneath the Kahktang Thrust in the Bumthang region of Bhutan, where it is overridden by GHS gneisses in the hanging wall. This arrangement clearly distinguishes it from TSS rocks that crop out predominately north of the Tibet-Bhutan border, the Linshi klippe in northwest Bhutan, and the Radi klippe in south-east Bhutan, which is isolate in terms of map pattern.

- The recognition that the structurally lower part of the TSS in the Nikha Chu-Tang Chu -Pele La area contains near-recumbent north-verging fold nappes, and that this type of structural style is likely to be more prevalent than previously recognised. This folding provides a good structural explanation

for the predominance of higher stratigraphic carbonate-dominated TSS rocks in the north and near the STD, whereas psammite-dominated, lower stratigraphic TSS rocks are dominant in the south.

- The identification of a sheared basal contact to this internally-folded body of TSS rocks that corresponds to the STD, from the north (Nikha Chu) to the south (Sure), contradicting previous interpretations that the southern part of this mass lies conformably on GHS rocks (Long & McQuarrie 2010).

- The discovery and prevalence of leucogranite emplaced at the basal TSS contact in many locations from the Nikha Chu to the large mass 20-30km south of Wangdue Phodrang, with the Gophu La granite being of comparable size to the Monlakarchung-Passalum body in north central Bhutan, one of the largest in the Himalaya.

- The extension of the main body of Paro metasediments to the east around Wangdue Phodrang as an east-dipping mass of rock beneath the MCT.

- Improved evidence for previously proposed, large-scale late folding in E-W and later N-S orientations, producing the elongate dome and basin structures that are responsible for the first order map pattern of Bhutan defined by the TSS and GHS rocks and their bounding faults.

Age of igneous rocks

Ash bed within TSS quartzite

A 10 cm thick meta-volcanic ash bed was sampled at locality LG-09-21 within bedded buff quartzite near Zhemgang (Figure 11a, b; see Figure 2 for location). We tentatively assign the quartzite with its ash bed to the Singhi Formation at the base of the Pele La Group that immediately overlies the Chekha Formation (Tangri & Pande 1995), based on its cross bedding, location and association with volcanic horizons. The pale cream-coloured ash bed forms a continuous, bedding-parallel band across the outcrop, weathering more recessively than the quartzite beds above and below. Large (2 mm), randomly-oriented porphyroblasts of biotite are set in a fine-grained matrix of muscovite and quartz, with accessory titanite, zircon and magnetite.

ID-TIMS results

Zircons selected for analysis were primarily elongate (>3:1) clear crystals typical of volcanic zircons. Single grain chemically annealed zircon ID-TIMS results (Figure 11c, d; Table 3) show some scatter in ages attributed to Pb-loss (z2, z4 and z12) and minor inheritance (z11, z8 and z15). Four analyses (z2, z3,

z4 and z12) define a linear array with intercepts at 74 ± 11 Ma and 499.8 ± 3.7 Ma, MSWD = 2.7. The scatter indicated by the MSWD is slightly higher than expected for a sample population of four, most likely reflecting a mixture of residual modern day and older (Himalayan) Pb-loss. Three additional analyses plot at slightly older ages off Concordia, consistent with very minor older inheritance. The most concordant analysis (z3) records a $^{207}Pb/^{206}Pb$ date of 497.2 ± 3.3 Ma, in agreement with the upper-intercept date. We interpret the 4-point upper intercept date of 499.8 ± 3.7 Ma as the age of zircon crystallisation on eruption and subsequent rapid deposition of the ash bed.

Granitic dykes

U-Pb data for three cross-cutting granites (LG-09-7A, LG-10-33 and LG-10-87) are presented in detail (Figure 12, Tables 4, 5).

Sample LG-09-7A is a coarse-grained, undeformed pegmatite sampled from a ~1 m wide dyke that cross-cuts the ductile foliation of an orthogneiss in the middle part of the GHS just west of Trongsa. The pegmatite contains mainly K-feldspar, plagioclase, quartz and muscovite.

Sample LG-10-33 was collected from a 2 m wide, medium-grained, leucocratic, peraluminous dyke that is homogeneous and undeformed, lacking any internal fabric. The dyke cuts TSS limestone in the upper Nikha Chu valley as a planar sheet with a north-south strike. The dyke cross-cuts tight, recumbent folds within carbonate strata. LG-10-33 contains plagioclase, microcline and quartz, with 5% tourmaline and 2 % muscovite. Leucogranite dykes cutting folds are shown in Figure 4f, about 1km from this locality.

LG-10-87B is a medium- to coarse-grained metaluminous granite sample from a ~1 m wide, cross-cutting dyke intruded into TSS calc-silicates near Chukha (Figure 9). The dyke is composed mainly of quartz (35%) and feldspar (both plagioclase and K-feldspar), with minor tourmaline (2%) and biotite (1%). It is somewhat altered (containing 7% chlorite) and has little internal fabric.

LA-ICP-MS results

Data for the three cross-cutting samples are presented on concordia plots (Figure 12b-d) and in Tables 4 and 5. Where possible, data were collected entirely within oscillatory-zoned portions. Some analyses targeted zircon tip and outer thin rims, but also included variable amounts of other zones, leading to mixed ages.

Most zircon grains from GHS sample LG-09-7A (Figure 12a) are 100 – 300 µm wide fragments of euhedral crystals. Most grains are dark with no CL-bright, xenocrystic cores. Most crystals show oscillatory zoning, with some convolute and patchy zoning that was avoided during analysis. A

regression of eight analyses in sample LG-09-7A yielded an intercept age of 13.20 ± 0.28 Ma, MSWD of 4.4. A further group of 3 near-concordant analyses yielded a regressed intercept of c. 18.1 Ma. Other discordant analyses probably represent mixing between different growth generations.

Zircon grains in sample LG-10-33 (Figure 12a) are moderately elongate (average elongation ratio of ~3). Roughly 25% have CL-bright cores; other grains and thin (5 – 100 μm) rims are mainly dark in CL. All crystals show oscillatory zoning, with some convolute zoning that was avoided during analysis. Two analyses of the cores of zircon grains in sample LG-10-33 lie off Concordia projecting to ~500 Ma. Eight analyses of the rims and dark grains give a regressed intercept age of 17.80 ± 0.18 Ma, MSWD of 1.4. Two analyses of the rims plot close to Concordia giving a regressed intercept age of 22.27 ± 0.60 Ma, MSWD of 3.2; these discordant data probably represent mixtures of material from different age zones. This demonstrates that early folds are older than 17.6 Ma.

Zircon grains in sample LG-10-87B (Figure 12a) are moderately elongate (average elongation ratio of ~3). Roughly a third of imaged grains have bright cores in CL, with variable zoning. 5 – 50 μm wide rims are generally dark in CL with clear oscillatory zoning. Four analyses of the cores in grains in sample LG-10-87B lie off Concordia projecting to ~1500 Ma while another two project to 2000 Ma or more. Ten analyses of the rims and dark grains give a regressed intercept age of 17.89 ± 0.48 Ma, MSWD of 4.7.

The ~18 Ma and ~13 Ma ages are interpreted as dating crystallisation of these cross-cutting granites. In particular these ~18 Ma ages demonstrate that early deformation within TSS units is ~18 Ma old or older. Igneous events continued as young as ~13 Ma within the lower GHS units.

Discussion

The TSS in central Bhutan: extent, age, basal contact and internal structure

Our new observations on the outcrop occurrences of TSS rocks dramatically increase the TSS outcrop area in central Bhutan. Accordingly, our TSS-GHS contact near Sure is mapped in a similar position to that of Gansser (1983), but ~10 km further south from the analogous boundary as published by Long *et al.* (2011a). Our contact is based on 1) evident shear displacement along this contact; 2) a change in metamorphic grade in excess of a plausible lithostatic gradient. We have considered the metamorphic P-T data of Corrie *et al.* (2012) which provides quantitative data on metamorphism. When their data are split into separate southern transects and one shifts the apparent boundary between their upper and lower GHS towards the south (towards the GHS gneisses) by a few hundred metres (corresponding to our GHS-TSS contact), it is entirely logical to infer a relatively abrupt step in metamorphic P and T

conditions (~70 °C and ~2.5 kbar) at exactly the same location (LG-09-43) on the Sure-Zhemgang transect as our mapped TSS-GHS contact (Corrie *et al.* 2012; between their samples BU08-76 and BU08-77). This P-T step is best explained by inhomogeneous attenuation (as opposed to the uniform flattening interpretation of Corrie *et al.*, 2012) of metamorphic isograds due to normal-sense shear strain across the STD that we describe. We stress ours is simply a different interpretation of the same quantitative data. In addition, we note that schists of similar grade to the garnet-staurolite schists comprising the basal TSS in this study occur in analogous structural positions in eastern Bhutan (Kellett *et al.* 2010; Chambers *et al.* 2011), Himachal Pradesh (Chambers *et al.* 2009) and central Nepal (Webb *et al.* 2011). The former two occurrences exhibit evidence for syn- to post-kinematic metamorphic mineral growth, similar to the randomly-oriented staurolite at locality LG-09-9. However, rocks of similar grade in this structural position have also been assigned to the upper GHS (e.g., Larson *et al.* 2010; Long and McQuarrie 2010), or an intermediate unit (Jessup *et al.* 2008). We conclude that the recent interpretation of stratigraphic conformity between the basal TSS and the underlying high grade GHS (e.g. Long and McQuarrie, 2010) is not supported, largely because these authors considered schists of the basal TSS to represent upper GHS rocks and therefore assessed a TSS-GHS 'contact' that we argue lies wholly within the Chekha Fm (lower TSS).

It is also difficult to reconcile our observations of a tightly-folded (in part nearly recumbent) TSS section with the depositional GHS/TSS contact model of Long & McQuarrie (2010) in southern Bhutan, unless it can be demonstrated that the basal stratigraphic contact is itself isoclinally folded. We have described the abundance of cleavage/foliation related to tight to isoclinal, north- or northwest-vergent folds on cm to km scales in the north, and that these early folds are older than a 17.8±0.2 Ma cross-cutting granite. These early, near-recumbent folds exert an important control on outcrop of lithologies in the TSS (Figure 6b).

North-verging folds have not been described from Bhutan on this scale before, but similar N-vergent folds in the Nepal Himalaya (Kellett & Godin 2009 and references therein) were dated using K-Ar on white mica to 30-25 Ma (Crouzet *et al.* 2001, 2007). Kellett & Godin 2009 suggest that these north-verging folds could have been the result of: (1) gravity-driven sliding along the STD (Burchfiel *et al.* 1992); (2) an early period of compression and crustal thickening (Brown & Nazarchuk 1993) during the Oligocene being transposed into the STD (Godin *et al.* 1999; Searle 2010); (3) folds forming during extrusion of the GHS in the Oligocene before the STD was active (c. 22 Ma; Carosi *et al.* 2007); (4) early compressional folds modified by horizontal stretching flow of the GHS (Kellett & Godin 2009).

585 Geometrically, these north-verging folds in the northern TSS of Bhutan might result from southward
586 extrusion of the underlying GHS rocks, in a north-verging shear couple, which would imply that the folds
587 are partly contemporaneous with the early stages of movement on the north-verging STD, rather than
588 due to contraction during the earlier thickening of the TSS in Eo-Himalayan time (>35 Ma). Other
589 interpretations are possible with the STD and folds unrelated, implying nappe formation before STD
590 movement. The early north-verging folds in the upper Nikha Chu appear compatible with either of
591 these origins, as both can provide explanations for (1) the kinematic congruence of these folds, (2) the
592 downward tightening of the folds towards the directly underlying STD, and (3) the observation that the
593 STD here is a ductile zone of shear that is not itself folded. We note that few of the leucogranites that
594 adorn the GHS-TSS contact extend far into the deformed TSS hanging wall, and that only two in this
595 study were deformed. All but one of the leucogranites adjacent to the STD, whether cross-cutting or
596 structurally concordant, yielded ages of ~17 – 20 Ma. We infer that TSS nappe structures might have
597 formed earlier in the STD motion and that leucogranite generation accompanied the latter stages of
598 STD motion around 18 – 20Ma ago.

599 The age of 500±4 Ma for the volcanic ash bed within quartzite of the TSS is approximately
600 commensurate with other age estimations for the Pele La Formation. Hughes *et al.* (2011) determined
601 depositional ages for the Quartzite Formation (uppermost Pele La Group) of ca. 493 Ma (Stage 9 of the
602 Furongian Epoch, using trilobite fossil evidence) and 487 ± 8 Ma (youngest detrital zircon ages),
603 marginally younger than the age calculated in this study. This age relationship is consistent with our
604 assignment of the ash bed to the Singhi Formation (lowermost Pele La Gp.), though detailed logging and
605 stratigraphic analysis would be required to confirm this supposition – data that has yet to be acquired
606 and which may be unobtainable given the limited outcrop and extensive deformation. Two detrital
607 zircons from samples of the Chekha or the upper GHS unit of Long and McQuarrie (2010) are pertinent.
608 A youngest detrital zircon age peak of 514 Ma from the underlying Chekha Formation of the Tang Chu
609 region (sample BU10-94 in McQuarrie *et al.* 2013) is also broadly consistent with the ash bed age. As
610 McQuarrie *et al.* (2013) caution, much of the TSS stratigraphy in Bhutan has been mapped on
611 lithological grounds (in the absence of fossil evidence), and detrital zircon studies are revealing
612 numerous inconsistencies in the mapped succession. While some variability is expected due to quirks of
613 sediment provenance, it is probable that some strata have been wrongly assigned using lithological
614 criteria. Long and McQuarrie (2010) also report in their sample Z60 of their upper GHS unit ~460 Ma as
615 the age of the youngest zircon. However, according to their 'continuous stratigraphic section'
616 interpretation of TSS-GHS rocks south of Zhemgang, their upper GHS (equivalent to our basal TSS) has
617 to be younger than ~460Ma, clearly contradicted by our 500±4 Ma age for the ash bed within putative

TSS of the Chekha/Singi formation. This contradiction can only be explained by a much different interpretation of the ~460 Ma zircon analytical data (perhaps underestimated due to discordance/Pb loss), or by there being no stratigraphic continuity between the upper GHS and their TSS Chekha formation of Paleozoic age. Our explanation is that while some ambiguity of the analytical data is likely, their sample Z60 belongs to the TSS and that detailed mapping is not good enough to correlate the two localities due to structural complexity. This discussion, detrital zircon data of Long and McQuarrie (2010) and McQuarrie *et al.* (2013), and our data on the ash bed, suggest strongly that the TSS, including the Singi and Chekha formations is Palaeozoic in age, and does not include any rocks of demonstrably Neoproterozoic age.

Volcanism at ~500 Ma is sparsely documented in Himalayan strata. Bhargava (2008) ascribed the few occurrences (including the calc-alkaline Singhi Volcanics of Bhutan) to rifting. Notwithstanding biasing of the ash bed's composition by sediment particles (likely mostly quartz), its composition supports an affinity with rhyolitic-dacitic layers within the Singhi volcanic suite near Chendebji (Tangri & Pande 1995), approximately 30 km north-west of the ash bed dated in this study. Numerous granitic intrusions in the Himalaya have yielded crystallisation ages of between ~450 and ~560 Ma (Miller *et al.* 2001 and references therein), contemporaneous with widespread evidence for Cambro-Ordovician magmatism, deformation and exhumation along the northern Indian margin (Cawood *et al.* 2007; Gehrels *et al.* 2011). So the ash bed dated in this study could represent the extrusive expression of this regional event.

Location of the Kakhtang Thrust

This study found no field evidence (such as abrupt juxtaposition of different rock types or metamorphic grades, or a zone of focused high strain or brittle fracturing) supporting the hypothesis that the Kakhtang Thrust cuts the GHS section south of the Gophu La granite, as has been previously implied (e.g. Grujic *et al.* (2002); Long *et al.* 2011a). In fact the Gophu La granite's southern contact dips beneath the TSS section as a zone of shear correlated with the structural contact (STD) at the base of the TSS section. The trace of the Kakhtang Thrust must therefore track north-westerly from the Bumthang region along the northern mapped extent of metamorphosed TSS rocks. This suggests that it may project north-westwards towards the northern part of the Gophu La granite, eventually joining with the Laya Thrust of Warren *et al.* (2011), though there is no mapping to confirm this.

Conclusions: Geological features of central Bhutan

This study has contributed new information and reinterpreted considerable existing information concerning the geology and tectonics of central Bhutan. Our main contributions are:

1. The TSS strata in central Bhutan are more widespread than previously mapped, forming a continuous outcrop that reaches from the Gophu La granite at the head of the Nikha Chu to within ~2 km of the MCT south of Zhemgang, and further west in a synclinal keel near Chukha. This TSS outcrop is rooted beneath the Kahktang Thrust in the Bumthang region of Bhutan. Our mapping has also revised the eastern margin of the existing Paro window to the east near Wangdue Phodrang.

2. Sheets of leucogranite emplaced along or just beneath the STD are more extensive than previously mapped. These granites are associated with the STD as far south as the latitude of Zhemgang; in places they are very extensive, rivalling in area the larger leucogranites of the entire Himalaya.

3. The extensive, allochthonous sheet of TSS rocks is soled by a wholly ductile tectonic contact, characterised by top-to-the-north or northwest shear sense. Metamorphic mineral growth in the basal TSS adjacent to this shear zone in part shows a syn- to post-kinematic relationship with the shear fabric, suggesting that heat flow upwards outlasted deformation, consistent with an extensional fault correlated with the STD.

4. Tight folding is observed throughout the TSS allochthon on scales from centimetres to kilometres, commonly with associated low-dipping axial-planar cleavage formation. Leucogranite intrusions that cross-cut these structures crystallised at 17.8 ± 0.2 and 17.9 ± 0.5 Ma, providing a minimum age for the folding event. Changing bedding-cleavage relationships indicate the presence of 100 m scale folds in many areas. Moreover, large-scale inverted sequences and fold closures in the Nikha Chu-Thampe Chu area define the closure of a major, north-vergent fold nappe in the TSS.

5. The internal folding in the TSS allochthon and its ductile, tectonic basal contact are both inconsistent with the notion that the TSS overlies the GHS in stratigraphic continuity in southern Bhutan.

6. An ash bed likely within the lower psammitic Singhi Formation of the Pele La Group in the TSS has been dated by U-Pb zircon at 500±4 Ma (mid-Cambrian). This represents the first firm isotopic age constraint for the lower TSS in the eastern Himalaya, and with previous detrital zircon and fossil

dates within the TSS, including the Chekha Formation, suggests that the TSS in Bhutan mainly Palaezoic in age.

Chronological Summary of selected tectonic events

We summarise the following broadly sequential events in Bhutan:

- Folding during greenschist facies metamorphism of TSS strata to form recumbent large scale folds, some north-vergent, prior to 18-20 Ma, in one or more major tectonic events;
- Formation of ductile south-directed fabrics within GHS during high grade metamorphism as part of its transport to the south on the Main Central Thrust (MCT) during the Miocene;
- Movement on the extensional north-directed STD, juxtaposing TSS strata with the GHS, involving an attenuation of isograds and inhomogeneous thinning along this zone, and in many places causing late- to post-kinematic mineral growth, in part accompanied by leucogranite intrusion dating to ~18-20 Ma, as sheets in close proximity to the STD;
- Thrusting of the GHS onto the deformed TSS, also post-dating the STD juxtaposition of TSS and GHS, along the out-of-sequence Kahktang Thrust, depressing the TSS within its footwall during the period 16-10 Ma;
- Upright folding along E-W axes of the entire tectonic stack of units in Bhutan;
- Upright ~N-S folding of previous units and structures;
- Initiation of the Main Boundary Thrust at approximately 10 Ma.

These events are not exhaustive but outline instead some of the main tectonic events. This study's main contribution is in presenting a major revision to all previously published geological maps of Bhutan that resolves many of the apparent or real inconsistencies amongst the many Bhutan geological studies published to date, and which identifies major early structures not previously described. Our map appears to be consistent with a large body of data and observation and explains why the map pattern of Bhutan is so distinctive relative to other regions of the Himalaya. We predict that these new data and map interpretation will encourage subsequent studies to examine the extent of early nappe-like structures in TSS rocks, map more systematically in areas that have not been very accessible in the past, identify problems with our work and propose new solutions, and encourage more attention to the mapping of geology in a manner inspired by the likes of Gansser and Bhargava while using all of the modern remote sensing and other geophysical, structural and petrochemical tools now available.

Acknowledgments

We would like to thank Ugyen Wangda (Head/Chief Geologist), Geological Survey of Bhutan for assistance and support in Bhutan. Nyima Om of Namsay Adventures is thanked for excellent logistical arrangements, Namgay and Tashi as guides, Tilly for driving and Laura Bracciali for field assistance. We would like to thank Nick Roberts and Dan Condon for U-Pb dating support at NIGL, Tony Miladowski for help with CL imaging at BGS and Adrian Wood for help with rock crushing and mineral separation at NIGL/BGS. This research was conducted by LVG under the BGS BUFI initiative (project S168) with partial funding for the project by the British Geological Survey. Isotope analyses were supported by facilities' access grant IP-1177-0510 awarded by the Natural Environment Research Council.

References

Beaumont, C., Jamieson, R. A., Nguyen, M. H. & Lee, B. 2001. Himalayan tectonics explained by extrusion of a low-viscosity crustal channel coupled to focused surface denudation. *Nature* **414**(6865), 738-742.

Bhargava, O. N. 1995. The Bhutan Himalaya: A Geological Account. *Geological Survey of India Special Publication* **39**, Geological Society of India, Calcutta, 245 pp.

Bhargava, O. N. 2008. Palaeozoic successions of the Indian plate. In: *National Symposium on Geodynamics and Evolution of the Indian Shield – Through Time and Space.* Geological Society of India, 13-14.

Brown, R. L. & Nazarchuk, J. H. 1993. Annapurna detachment fault in the Greater Himalaya of Central Nepal. In: *Himalayan Tectonics* (edited by Treloar, P. J. & Searle, M. P.). *Geological Society of London Special Publication* **74**, 461-473.

Burchfiel, B.C. & Royden, L.H., 1985. North–south extension within the convergent Himalayan region. *Geology* **13**, 679– 682.

Burchfiel, B. C., Chen, Z., Hodges, K. V., Yuping, L., Royden, L. H., Changrong, D. & Jiene, X. 1992. The south Tibetan detachment system, Himalayan orogen: Extension contemporaneous with and parallel to shortening in a collisional mountain belt. *Geological Society of America Special Paper* **269**.

Burg, J.P., Brunel, M., Gapais, D., Chen, G.M., Liu, G.H., 1984. Deformation of leucogranites of the crystalline main central sheet in southern Tibet (China). *Journal of Structural Geology* **6**, 535–542.

Carosi, R., Montomoli, C. & Visonà, D. 2007. A structural transect in the Lower Dolpo: Insights on the tectonic evolution of Western Nepal. *Journal of Asian Earth Sciences* **29**(2), 407-423.

Cawood, P.A., Johnson, M.R.W. & Nemchin, A.A. 2007. Early Paleozoic orogenesis along the Indian margin of Gondwana: tectonic response to Gondwana assembly. *Earth and Planetary Science Letters* **255**, 70–84 http://dx.doi.org/10.1016/j.epsl.2006.12.006.

740 Chakungal, J., Dostal, J., Grujic, D., Duchêne, S., & Ghalley, K. S. 2010. Provenance of the Greater
741 Himalayan sequence: Evidence from mafic granulites and amphibolites in NW Bhutan.
742 *Tectonophysics*, **480**(1), 198-212.

743 Chambers, J., Caddick, M., Argles, T., Horstwood, M., Sherlock, S., Harris, N., Parrish, R. & Ahmad, T.
744 2009. Empirical constraints on extrusion mechanisms from the upper margin of an exhumed
745 high-grade orogenic core, Sutlej valley, NW India. *Tectonophysics* **477**(1-2), 77-92.

746 Chambers, J., Parrish, R., Argles, T., Harris, N. & Horstwood, M. 2011. A short-duration pulse of ductile
747 normal shear on the outer South Tibetan detachment in Bhutan: Alternating channel flow and
748 critical taper mechanics of the eastern Himalaya. *Tectonics* **30**(2), TC2005.

749 Condon, D., Schoene, B., Bowring, S., Parrish, R., Mclean, N., Noble, S. & Crowley, Q. 2007. EARTHTIME:
750 Isotopic tracers and optimized solutions for high-precision U-Pb ID-TIMS geochronology. In:
751 *AGU Fall Meeting Abstracts* **1**, 06.

752 Corrie, S. L., Kohn, M. J., McQuarrie, N. & Long, S. P. 2012. Flattening the Bhutan Himalaya. *Earth and*
753 *Planetary Science Letters* **349**, 67-74.

754 Cottle, J. M., Horstwood, M. S. A. & Parrish, R. R. 2009. A new approach to single shot laser ablation
755 analysis and its application to in situ Pb/U geochronology. *Journal of Analytical Atomic*
756 *Spectrometry* **24**, 1355-1363. doi: 10.1039/b821899d.

757 Crouzet, C., Dunkl, I., Paudel, L., Arkai, P., Rainer, T., Balogh, K. & Appel, E. 2007. Temperature and age
758 constraints on the metamorphism of the Tethyan Himalaya in Central Nepal: A multidisciplinary
759 approach. *Journal of Asian Earth Sciences* **30**(1), 113-130.

760 Crouzet, C., Gautam, P., Appel, E. & Schill, E. 2001. Discussion on new paleomagnetic results from
761 Tethyan Himalaya (Western Nepal): tectonic and geodynamic implications. *Journal of Asian*
762 *Earth Sciences* **19**(3A), 11.

763 Daniel, C. G., Hollister, L. S., Parrish, R. R. & Grujic, D. 2003. Exhumation of the Main Central Thrust from
764 lower crustal depths, eastern Bhutan Himalaya. *Journal of Metamorphic Geology* **21**(4), 317-
765 334.

766 Davidson, C., Grujic, D. E., Hollister, L. S. & Schmid, S. M. 1997. Metamorphic reactions related to
767 decompression and synkinematic intrusion of leucogranite, High Himalayan Crystallines,
768 Bhutan. *Journal of Metamorphic Geology* **15**(5), 593-612.

769 Edwards, M. A. & Harrison, T. M. 1997. When did the roof collapse? Late Miocene north-south
770 extension in the high Himalaya revealed by Th-Pb monazite dating of the Khula Kangri granite.
771 *Geology* **25**(6), 543.

772 Edwards, M. A., Pêcher, A., Kidd, W. S. F., Burchfiel, B. C., & Royden, L. H. 1999. Southern Tibet
773 Detachment System at Khula Kangri, Eastern Himalaya: A Large-Area, Shallow Detachment
774 Stretching into Bhutan? *The Journal of Geology*, **107**(5), 623-631.

775 Gansser, A. 1964. *Geology of the Himalayas.* Interscience Publishers, London.

776 Gansser, A. 1983. *Geology of the Bhutan Himalaya.* Birkhauser Verlag, Basel.

777 Gehrels, G.E., Kapp, P., DeCelles, P.G., Pullen, A., Blakey, R., Weislogel, A., Ding, L., Guynn, J., Martin, A.,
778 McQuarrie, N. & Yin, A. 2011. Detrital zircon geochronology of pre-Tertiary strata in the
779 Tibetan-Himalayan orogeny. *Tectonics* **30**, TC5016 http://dx.doi.org/10.1029/2011TC002868.

780 Godin, L., Brown, R. L., Hanmer, S. & Parrish, R. 1999. Back folds in the core of the Himalayan orogen:
781 An alternative interpretation. *Geology* **27**(2), 151-154.

782 Godwin-Austen, H. H. 1868. Note on geological structure of the country near foothills in the western
783 Bhutan Dooars. *Jour. Asiatic Soc. Benf* **37**(Pt 1).

784 Grasemann, B., Fritz, H. & Vannay, J.C. 1999. Quantitative kinematic flow analysis from the Main Central
785 Thrust Zone (NWHimalaya, India): implications for a decelerating strain path and the extrusion
786 of orogenic wedges. *Journal of Structural Geology* **21**, 837–853.

787 Griesbach C.L. 1891. *Geology of the Central Himalaya.* Geological Survey of India Memoir **XXIII**, 1-232.

788 Grujic, D., Hollister, L. S. & Parrish, R. R. 2002. Himalayan metamorphic sequence as an orogenic
789 channel: insight from Bhutan. *Earth and Planetary Science Letters* **198**(1-2), 177-191.

790 Grujic, D., Warren, C. J. & Wooden, J. L. 2011. Rapid synconvergent exhumation of Miocene-aged lower
791 orogenic crust in the eastern Himalaya. *Lithosphere* **3**(5), 346.

792 Grujic, D., Casey, M., Davidson, C., Hollister, L. S., Kündig, R., Pavlis, T. & Schmid, S. 1996. Ductile
793 extrusion of the Higher Himalayan Crystalline in Bhutan: evidence from quartz microfabrics
794 *Tectonophysics* **260**, 21-43.

795 Harris, N. & Massey, J. 1994. Decompression and anatexis of Himalayan metapelites. *Tectonics* **13**,
796 1537-1546.

Hayden, H. H. 1907. *The Geology of the Provinces of Tsang and U in Central Tibet*. Geological Survey of India Memoir.

Heim, A. 1921. *Geologie der Schweiz. 11. Die Schweizer Alpen.* Tauchnitz, Leipzig.

Heim, A., & Gansser, A., 1939, *Central Himalaya Geological Observations of the Swiss Expedition 1936*. Zurich, Gebrüder Fretz, 246 p.

Hodges, K.V., Parrish, R.R., Housh, T.B., Lux, D.R., Burchfiel, B.C., Royden, L.H., & Chen, Z. 1992. Simultaneous Miocene extension and shortening in the Himalayan orogen. *Science* **258**, 1446–1470.

Hollister, L. S. & Grujic, D. 2006. Pulsed channel flow in Bhutan. In: *Channel Flow, Ductile Extrusion and Exhumation in Continental Collision Zones* (edited by: Law, R. D., Searle, M. P., & Godin, L.) *Geological Society of London Special Publication* **268**, 415-423.

Hughes, N. C., Myrow, P. M., McKenzie, N. R., Harper, D. A. T., Bhargava, O. N., Tangri, S. K., Ghalley, K. S. & Fanning, C. M. 2011. Cambrian rocks and faunas of the Wachi La, Black Mountains, Bhutan. *Geological Magazine* **148**(3), 351-379.

Jaffey, A., Flynn, K., Glendenin, L., Bentley, W. C. & Essling, A. 1971. Precision Measurement of Half-Lives and Specific Activities of ^{235}U and ^{238}U. *Physical Review C* **4**(5), 1889.

Jangpangi, B. S. 1974. Stratigraphy and tectonics of parts of eastern Bhutan. *Himalayan Geology* **4**, 117-136.

Jessup, M.J., Cottle, J.M., Searle, M.P., Law, R.D., Tracy, R.J., Newell, D.L., and Waters, D.J. 2008. P-T-t-D paths of the Everest Series schist, Nepal. *Journal of Metamorphic Geology* **26**, p. 717–739, doi:10.1111/j.1525-1314.2008.00784.x.

Kellett, D. A. & Godin, L. 2009. Pre-Miocene deformation of the Himalayan superstructure, Hidden valley, central Nepal. *Journal of Geological Society* **166**(2), 261.

Kellett, D. A., Grujic, D. & Erdmann, S. 2009. Miocene structural reorganization of the South Tibetan detachment, eastern Himalaya: Implications for continental collision. *Lithosphere* **1**(5), 259.

823 Kellett, D., Grujic, D., Warren, C., Cottle, J., Jamieson, R. & Tenzin, T. 2010. Metamorphic history of a
824 syn-convergent orogen-parallel detachment: The South Tibetan detachment system, Bhutan
825 Himalaya. *Journal of Metamorphic Geology* **28**(8), 785-808.

826 Larson, K.P., Godin, L., and Price, R.A. 2010. Relationships between displacement and distortion in
827 orogens: Linking the Himalayan foreland and hinterland in central Nepal. *Geological Society of*
828 *America Bulletin* **122**, 1116–1134, doi:10.1130/B30073.1.

829 LeFort, P., Vuney, M., Deniel, C. & France-Lanord, C. 1987. Crustal generation of the Himalayan
830 leucogranites. *Tectonophysics* **134**, 39– 57.

831 Long, S. & McQuarrie, N. 2010. Placing limits on channel flow: Insights from the Bhutan Himalaya. *Earth*
832 *and Planetary Science Letters* **290**(3-4), 375-390.

833 Long, S., McQuarrie, N., Tobgay, T., Grujic, D. & Hollister, L. 2011a. Geologic Map of Bhutan. *Journal of*
834 *Maps* **7**(1), 184-192.

835 Long, S., McQuarrie, N., Tobgay, T., Rose, C., Gehrels, G. & Grujic, D. 2011b. Tectonostratigraphy of the
836 Lesser Himalaya of Bhutan: Implications for the along-strike stratigraphic continuity of the
837 northern Indian margin. *Bulletin of the Geological Society of America* **123**(7-8), 1406.

838 Lugeon, M. 1902. Les grandes nappes de recouvrement des Alpes de Chablais et de la Suisse. *Bulletin de*
839 *la* Société *Géologique de France* (4)**1**, 723-825.

840 Mallet, F. R. 1875. On the geology and mineral resources of the Darjeeling district and the western
841 Duars. *Memoirs of the Geological Survey of India* **11**, 1-50.

842 Mattinson, J. M. 2005. Zircon U-Pb chemical abrasion ("CA-TIMS") method: combined annealing and
843 multi-step partial dissolution analysis for improved precision and accuracy of zircon ages.
844 *Chemical Geology* **220**(1), 47-66.

845 McQuarrie, N., Robinson, D., Long, S., Tobgay, T., Grujic, D., Gehrels, G. & Ducea, M. 2008. Preliminary
846 stratigraphic and structural architecture of Bhutan: Implications for the along strike
847 architecture of the Himalayan system. *Earth and Planetary Science Letters* **272**(1-2), 105-117.

848 McQuarrie, N., Long, S. P., Tobgay, T., Nesbit, J. C., Gehrels, G., & Ducea, M. N. 2013. Documenting
849 basin scale, geometry and provenance through detrital geochemical data: Lessons from the
850 Neoproterozoic to Ordovician Lesser, Greater, and Tethyan Himalayan strata of Bhutan.
851 *Gondwana Research* **23**,1491–1510

852 Miller, C., Thöni, M., Frank, W., Grasemann, B., Klötzli, U., Guntli, P. & Draganits, E. 2001. The early
853 Palaeozoic magmatic event in the Northwest Himalaya, India: source, tectonic setting and age
854 of emplacement. *Geological Magazine* **138**(3), 237-251.

855 Mottram, C., Argles, T., Harris, N., Parrish, R., Horstwood, M., Warren, C. & Gupta, S., 2014. Tectonic
856 interleaving along the Main Central Thrust, Sikkim Himalaya. *Journal of the Geological Society of*
857 *London* **171**, 255-268, doi: 10.1144/jgs2013-064.

858 Pilgrim, G. E. 1906. Notes on the geology of a portion of Bhutan. *Records of Geological Survey of India*
859 **34**, 22-30.

860 Ray, S., Bandyopadhyay, B. & Razdan, R. 1989. Tectonics of a part of the Shumar allochthon in eastern
861 Bhutan. *Tectonophysics* **169**(1-3), 51-58.

862 Richards, A., Parrish, R., Harris, N., Argles, T. & Zhang, L. 2006. Correlation of lithotectonic units across
863 the eastern Himalaya, Bhutan. *Geology* **34**(5), 341.

864 Schneider, C. & Masch, L. 1993. The metamorphism of the Tibetan series from the Manang area,
865 Marsyandi valley, central Nepal. In: Treloar, P.J., Searle, M.P. (Eds.), *Himalayan Tectonics*.
866 *Geological Society Special Publication* **74**, 357– 374.

867 Searle, M. P. 2010. Low-angle normal faults in the compressional Himalayan orogen; Evidence from the
868 Annapurna-Dhaulagiri Himalaya, Nepal. *Geosphere* **6**(4), 296-315.

869 Swapp, S. M. & Hollister, L. S. 1991. Inverted metamorphism within the Tibetan slab of Bhutan:
870 Evidence for a tectonically transported heat-source. *Canadian Mineralogist* **29**(4), 1019.

871 Tangri, S. K. & Pande, A. C. 1995. Tethyan sequence. In: The Bhutan Himalaya: A Geological Account:
872 *Geological Society of India Special Publication* (edited by Bhargava, O. N.) **39**, 109-142.

873 Termier, P. 1904. Les nappes des Alpes orientales et la synthèse des Alpes. *Bulletin de la* Société
874 *Géologique de France* (4)**3** 711-766.

875 Thomas, R., Jacobs, J., Horstwood, M., Ueda, K., Bingen, B. & Matola, R. 2010. The Mecubúri and Alto
876 Benfica groups, NE Mozambique: aids to unravelling ca. 1 and 0.5 Ga events in the east African
877 orogen. *Precambrian Research* **178**, 72-90.

878 Thomas, R. J., Roberts, N. M. W., Jacobs, J., Bushi, A. M., Horstwood, M. S. A. & Mruma, A. 2013.
879 Structural and geochronological constraints on the evolution of the eastern margin of the
880 Tanzania Craton in the Mpwapwa area, central Tanzania. *Precambrian Research* **224**, 671-689.

881 Tobgay, T., Long, S., McQuarrie, N., Ducea, M. N. & Gehrels, G. 2010. Using isotopic and chronologic
882 data to fingerprint strata: Challenges and benefits of variable sources to tectonic
883 interpretations, the Paro Formation, Bhutan Himalaya. *Tectonics* **29**(6), TC6023.

884 Warren, C. J., Grujic, D., Kellett, D. A., Cottle, J., Jamieson, R. A. & Ghalley, K. S. 2011. Probing the
885 depths of the India-Asia collision: U-Th-Pb monazite chronology of granulites from NW Bhutan.
886 *Tectonics* **30**(2), TC2004.

887 Webb, A.A.G., Schmitt, A.K., He, D., and Weigand, E.L. 2011. Structural and geochronological evidence
888 for the leading edge of the Greater Himalayan Crystalline complex in the central Nepal
889 Himalaya. *Earth and Planetary Science Letters* **304**, 483–495, doi:10.1016/j.epsl.2011.02.024.

890 Webb, A.A.G., Yin, A., & Dubey, C. S. 2013. U-Pb zircon geochronology of major lithologic units in the
891 eastern Himalaya: Implications for the origin and assembly of Himalayan rocks. *Geological*
892 *Society of America Bulletin* **125** (3/4) 499–522, doi: 10.1130/B30626.1

893 Wu, C., Nelson, K. D., Wortman, G., Samson, S. D., Yue, Y., Li, J., Kidd, W. S. F. & Edwards, M. A. 1998.
894 Yadong cross structure and South Tibetan Detachment in the east central Himalaya (89 -90).
895 *Tectonics* **17**(1), 28-45.

896 Yin, A. 2006. Cenozoic tectonic evolution of the Himalayan orogen as constrained by along-strike
897 variation of structural geometry, exhumation history, and foreland sedimentation. *Earth*
898 *Science Reviews* **76**(1-2), 1-131.

899 Yin, A., Dubey, C. S., Kelty, T. K., Gehrels, G. E., Chou, C. Y., Grove, M. & Lovera, O. 2006. Structural
900 evolution of the Arunachal Himalaya and implications for asymmetric development of the
901 Himalayan orogen. *Current Science* **90**(2), 195.

902 Yin, A., Dubey, C., Webb, A., Kelty, T., Grove, M., Gehrels, G. & Burgess, W., 2010a. Geologic correlation
903 of the Himalayan orogen and Indian craton: Part 1. Structural geology, U-Pb zircon
904 geochronology, and tectonic evolution of the Shillong Plateau and its neighboring regions in NE
905 India. *Geological Society of America Bulletin*, **122**(3-4), 336-359.

Yin, A., Dubey, C. S., Kelty, T. K., Webb, A. A. G., Harrison, T. M., Chou, C. Y. & Celerier, J., 2010b. Geologic correlation of the Himalayan orogen and Indian craton: Part 2. Structural geology, geochronology, and tectonic evolution of the Eastern Himalaya. *Geological Society of America Bulletin*, **122**, 360-395.

Figure Captions

Figure 1 Simplified map of Himalaya showing semi-continuous units and location of study area, modified from Mottram *et al.* (2014).

Figure 2 New map of Bhutan incorporating data from this study and showing sample locations. Compiled using information from this study and previous work of Gansser (1983); Bhargava (1995); Grujic *et al.* (2002, 2011); McQuarrie *et al.* (2008); Long and McQuarrie (2010); Long *et al.* (2011a, b); Tobgay *et al.* (2010); Chakungal *et al.* (2010); Edwards *et al.* (1999); Wu *et al.* (1998); Warren *et al.* (2011); Hollister & Grujic (2006); Kellett *et al.* (2009); Daniel *et al.* (2003); Davidson *et al.* (1997); Grujic *et al.* (1996); Kellett *et al.* (2010); Chambers *et al.* (2011); Swapp and Hollister (1991); Richards *et al.* (2006).

Figure 3 Evolution of interpretations of the GHS-TSS outcrops with time: a selection of published maps of Bhutan, redrawn and simplified for ease of comparison with this work. (**a**) from Gansser (1983); (**b**) from Grujic *et al.* (2002); (**c**) from McQuarrie *et al.* (2013); (**d**) from this study.

Figure 4 Strata and structure in the TSS.(**a**) Photograph of right way up TSS strata overlying the Gophu La leucogranite, looking ENE from Thampetso La (Figure 5); (**b**) Annotated sketch of the same view as part (a); (**c**) metre scale tightly folded bedding within carbonate unit at LG-10-31; (**d**) view to the east along side valley east of locality 22 showing carbonate-dominated stratigraphy, interpreted to be partly inverted; (**e**) multiple fold hinges on a 50 cm scale within carbonate unit at LG-10-32; (**f**) tight folds in phyllitic limestone 1.2 km south of locality LG-10-33. Locations shown in Figure 5. .

Figure 5 Structural map of the Nikha Chu – Thampe Chu area. Line A-B marks line of cross-section in Figure 6a.

Figure 6 (**a**) Cross-section along the line A-B in Figure 5. Unit colours as in Figure 5. (**b**) Schematic diagram of north-vergent fold nappe in the TSS of central Bhutan. The TSS units thin progressively northwards, but more pronounced variations in the proportions of quartzite and carbonate between different areas are a consequence of the folding.

Figure 7 Leucogranite relationships in central Bhutan. (**a**) Pale dykes of leucogranite, not visibly deformed, intruded into overlying micaceous TSS quartzite at LG-09-78: view westwards at ~8 m high cliff face; (**b**) intrusive margin of foliated leucogranite body at LG-09-12 interfingering with GHS paragneiss. For locations, see Figure 2.

Figure 8 Field evidence for shear sense in the GHS and TSS. (**a**) rotated boudins with asymmetric tails in sillimanite garnet GHS paragneiss at LG-09-102 near Semtokha showing top-to-the-south sense-of-shear; (**b**) sillimanite bearing paragneiss of the GHS at LG-09-6 showing s-c fabric sketched in (**c**) indicating top-to-the-south sense-of-shear; (**d**) garnet-staurolite schist LG-09-43, the base of the TSS near Sure showing s-c shear fabric sketched in (**e**) indicating top-to-the-north sense-of-shear; (**f**) quartzite at LG-09-43 showing an isolated fold verging to the north.

Figure 9 Geological map of Chukha region. Dashed grey line marks location of inferred large-scale synform.

Figure 10 Geological map of the Wangdue window and the eastern reaches of the Paro window. Dashed line marks location of inferred large-scale antiform.

Figure 11 ID-TIMS results for metavolcanic ash bed LG-09-21, with field photograph of ash bed included as inset (a). Dark flecks are randomly-oriented biotite porphyroblasts. Main figure: concordia plot of ID-TIMS results for ash bed.

Figure 12 (**a**) Cathodoluminescence images of representative zircons from cross-cutting leucogranites (LG-09-7A, LG-10-33 and LG-10-87b). Circles represent laser ablation spots, with corresponding dates, in zircon rims (dashed white circles) and cores (black circles). Numbers within or beside the spot indicate the analysis number referred to in Table 5. (**b**) Laser ablation U-Pb geochronology of zircon rims and cores for LG-09-7A. (**c**) Laser ablation U-Pb geochronology of zircon rims and cores for LG-10-33. (**d**) Laser ablation U-Pb geochronology of zircon rims and cores for LG-10-87b. Plots (b), (c) and (d) comprise a main Concordia plot of all analyses and an inset showing a Tera-Wasserburg plot of young rim analyses. Errors are depicted at 2σ. LG-10-33 analyses in bold are ignored in the calculation of ages for the two rims on the Tera-Wasserburg plot.

Table 1 *Summary criteria for determining lithotectonic affinity in Bhutan*

Table 2 *Summary criteria for identifying major shear zones in Bhutan*

Table 3 *U-Pb ID-TIMS data for the ashbed sample LG-09-21*

Table 4 *Characteristics and ages of igneous rocks dated in this study*

Table 5 *U-Pb LA-ICP-MS data for granite samples LG-09-7A, LG-10-33 and LG-10-87B*

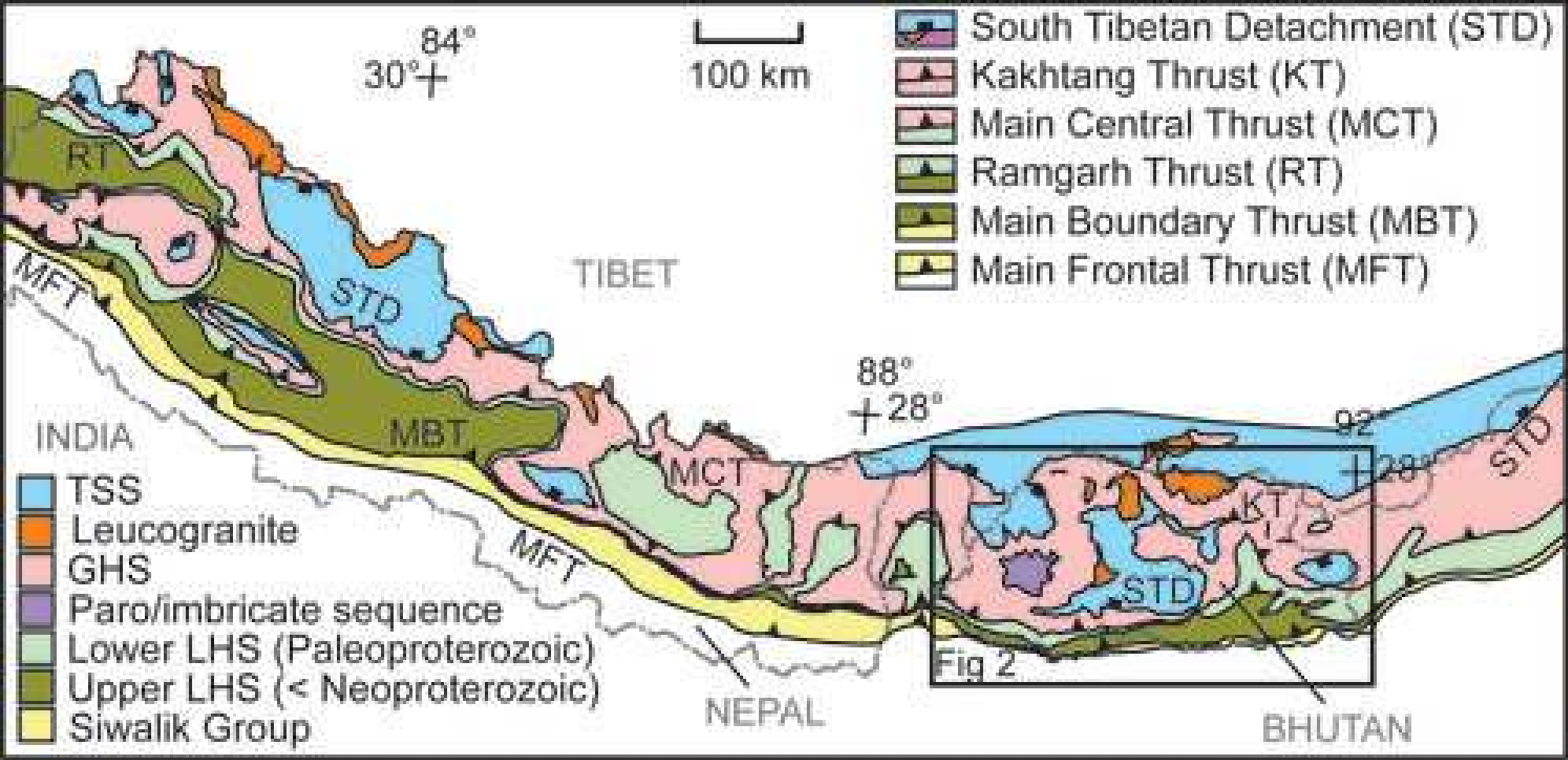
84°
30°
100 km
South Tibetan Detachment (STD)
Kakhtang Thrust (KT)
Main Central Thrust (MCT)
Ramgarh Thrust (RT)
Main Boundary Thrust (MBT)
Main Frontal Thrust (MFT)
TIBET
RT
MFT
STD
INDIA
MBT
MCT
88°
28°
92°
28°
KT
STD
MFT
A
A'
Fig 2
NEPAL
BHUTAN
TSS
Leucogranite
GHS
Paro/imbricate sequence
Lower LHS (Paleoproterozoic)
Upper LHS (< Neoproterozoic)
Siwalik Group

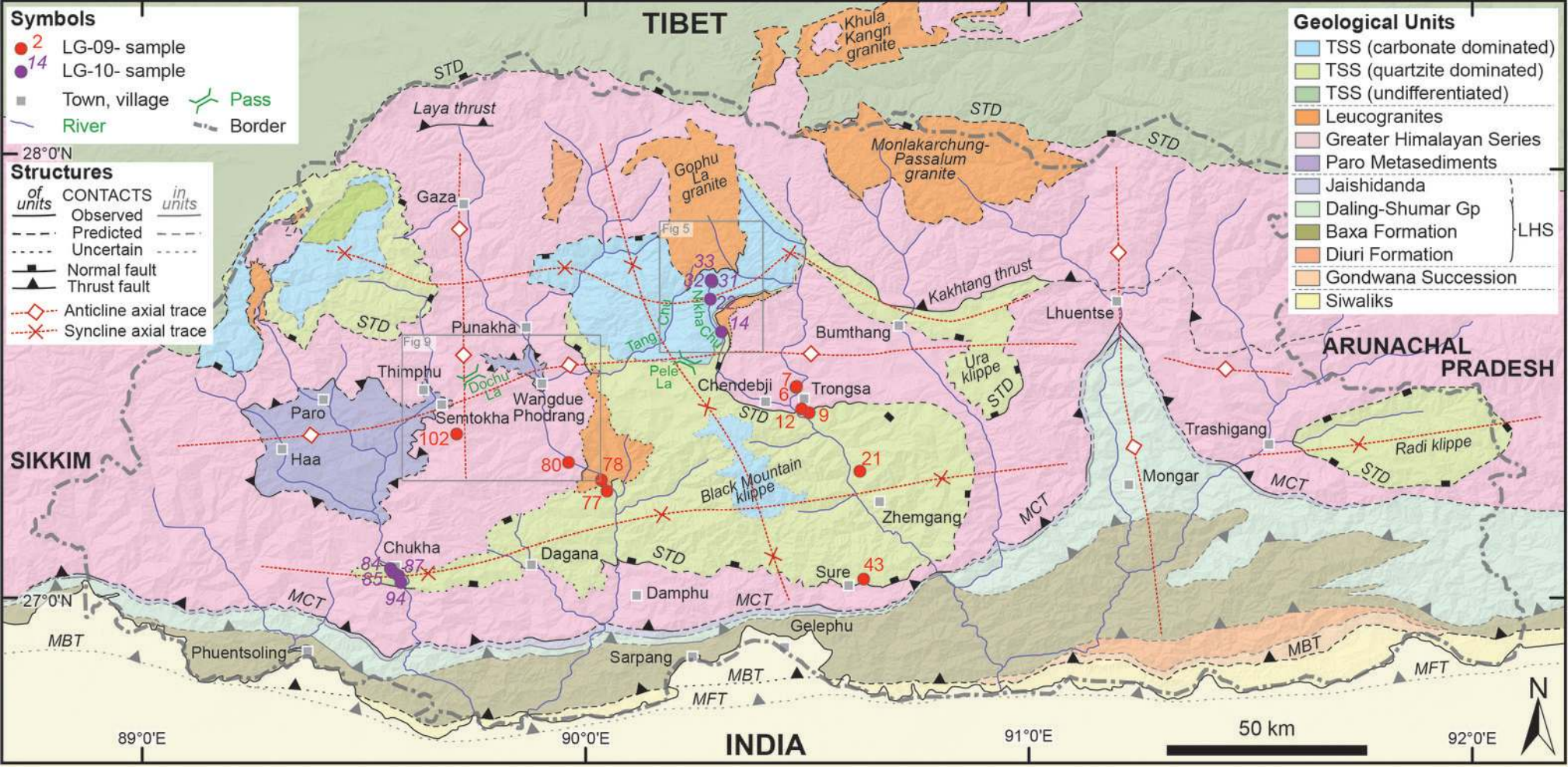
Symbols
2 LG-09- sample
14 LG-10- sample
Town, village
Pass
River
Border
Structures
CONTACTS
of units
in units
Observed
Predicted
Uncertain
Normal fault
Thrust fault
Anticline axial trace
Syncline axial trace
Geological Units
TSS (carbonate dominated)
TSS (quartzite dominated)
TSS (undifferentiated)
Leucogranites
Greater Himalayan Series
Paro Metasediments
Jaishidanda
Daling-Shumar Gp
Baxa Formation
Diuri Formation
LHS
Gondwana Succession
Siwaliks
TIBET
SIKKIM
ARUNACHAL PRADESH
INDIA
Khula Kangri granite
Laya thrust
Gophu La granite
Monlakarchung-Passalum granite
Kakhtang thrust
Ura klippe
Black Mountain klippe
Radi klippe
STD
MCT
MBT
MFT
Gaza
Punakha
Thimphu
Paro
Haa
Wangdue Phodrang
Semtokha
Dochu La
Pele La
Tang Chu
Mo Chhu
Bumthang
Chendebji
Trongsa
Lhuentse
Trashigang
Mongar
Zhemgang
Chukha
Dagana
Damphu
Sure
Gelephu
Sarpang
Phuentsoling
Fig 5
Fig 9
28°0'N
27°0'N
89°0'E
90°0'E
91°0'E
92°0'E
50 km
N

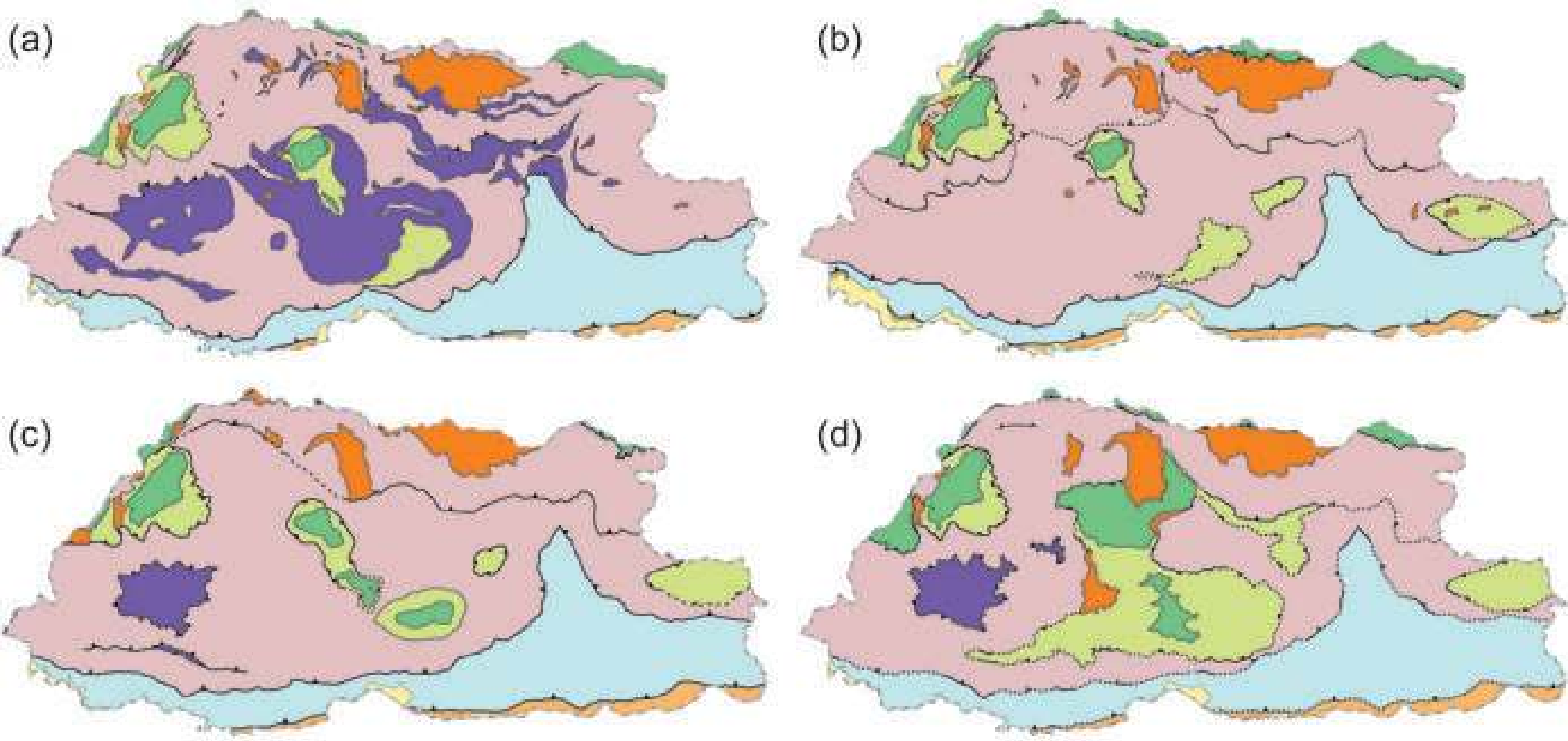
(a)
(b)
(c)
(d)
TSS (above Chekha Fm)
Chekha Fm
Tertiary leucogranite
GHS (undifferentiated)
Paro metasediments
LHS (undifferentiated)
Siwaliks
Quaternary
Lithological boundary
Normal fault (STD)
Thrust fault

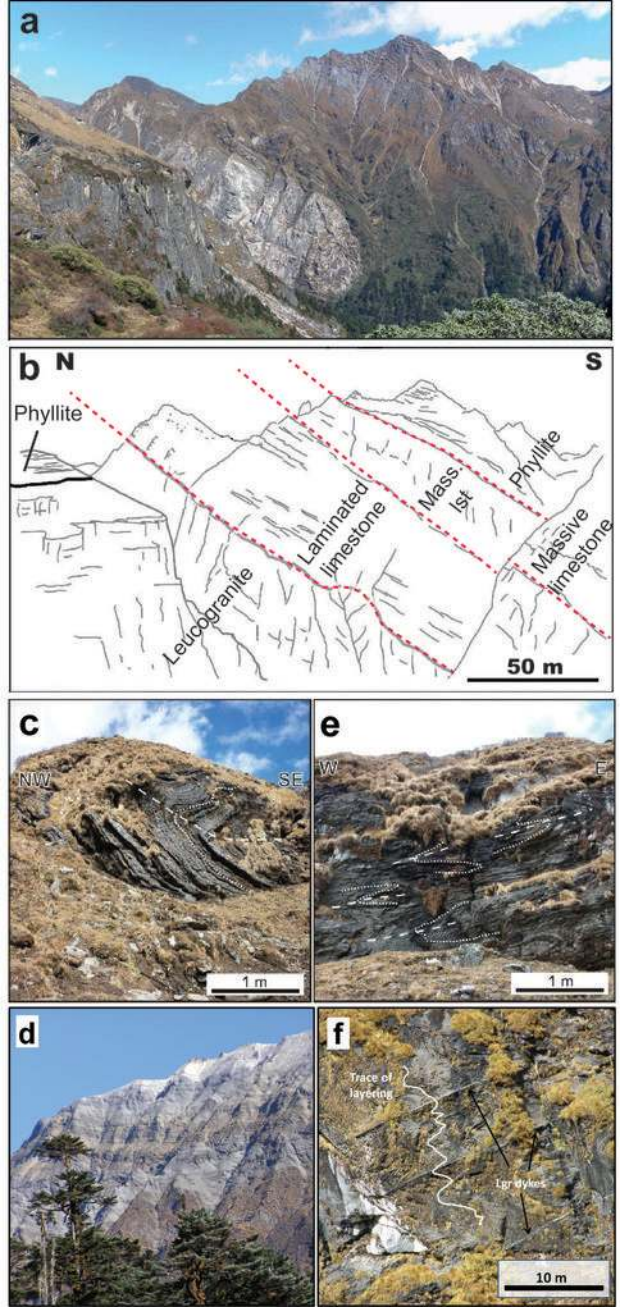
a
b
N
S
Phyllite
Laminated limestone
Mass. lst
Phyllite
Massive limestone
Leucogranite
50 m
c
NW
SE
1 m
e
W
E
1 m
d
f
Trace of layering
Lgr dykes
10 m

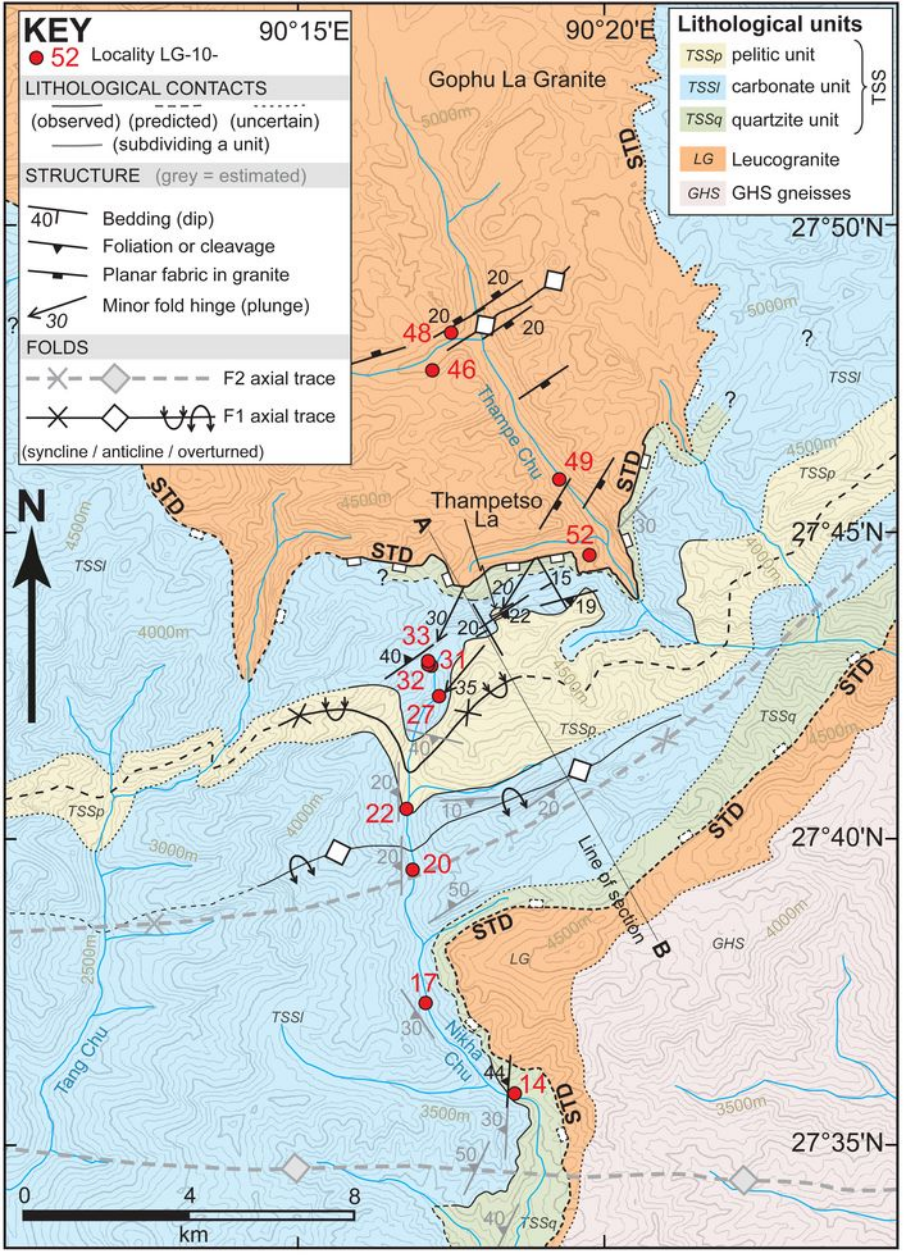
KEY
52 Locality LG-10-
LITHOLOGICAL CONTACTS
(observed) (predicted) (uncertain)
(subdividing a unit)
STRUCTURE (grey = estimated)
40 Bedding (dip)
Foliation or cleavage
Planar fabric in granite
30 Minor fold hinge (plunge)
FOLDS
F2 axial trace
F1 axial trace
(syncline / anticline / overturned)
90°15'E
90°20'E
27°50'N
27°45'N
27°40'N
27°35'N
Lithological units
TSSp pelitic unit
TSSl carbonate unit
TSSq quartzite unit
TSS
LG Leucogranite
GHS GHS gneisses
Gophu La Granite
STD
Thampe Chu
Thampetso La
A
B
Line of section
Tang Chu
Nikha Chu
TSSl
TSSp
TSSq
LG
GHS
48
46
49
52
33
31
32
27
22
20
17
14
N
0
4
8
km

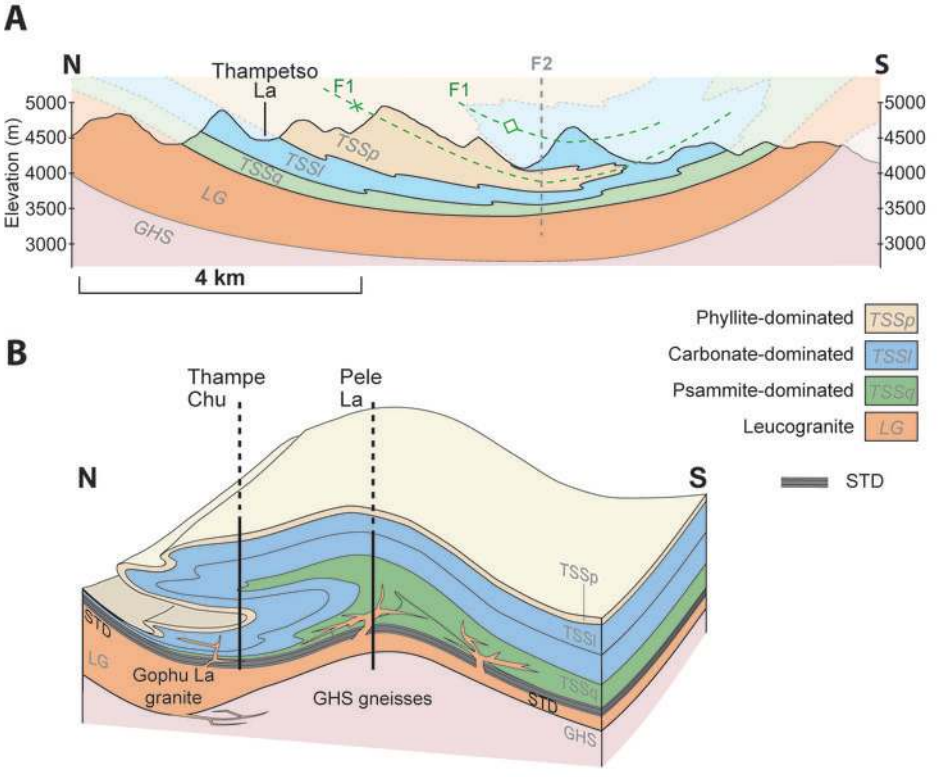
A
N
S
Thampetso La
F1
F1
F2
5000
4500
4000
3500
3000
Elevation (m)
TSSp
TSSl
TSSq
LG
GHS
4 km
B
Thampe Chu
Pele La
N
S
TSSp
TSSl
TSSq
STD
LG
Gophu La granite
GHS gneisses
STD
GHS
Phyllite-dominated TSSp
Carbonate-dominated TSSl
Psammite-dominated TSSq
Leucogranite LG
STD

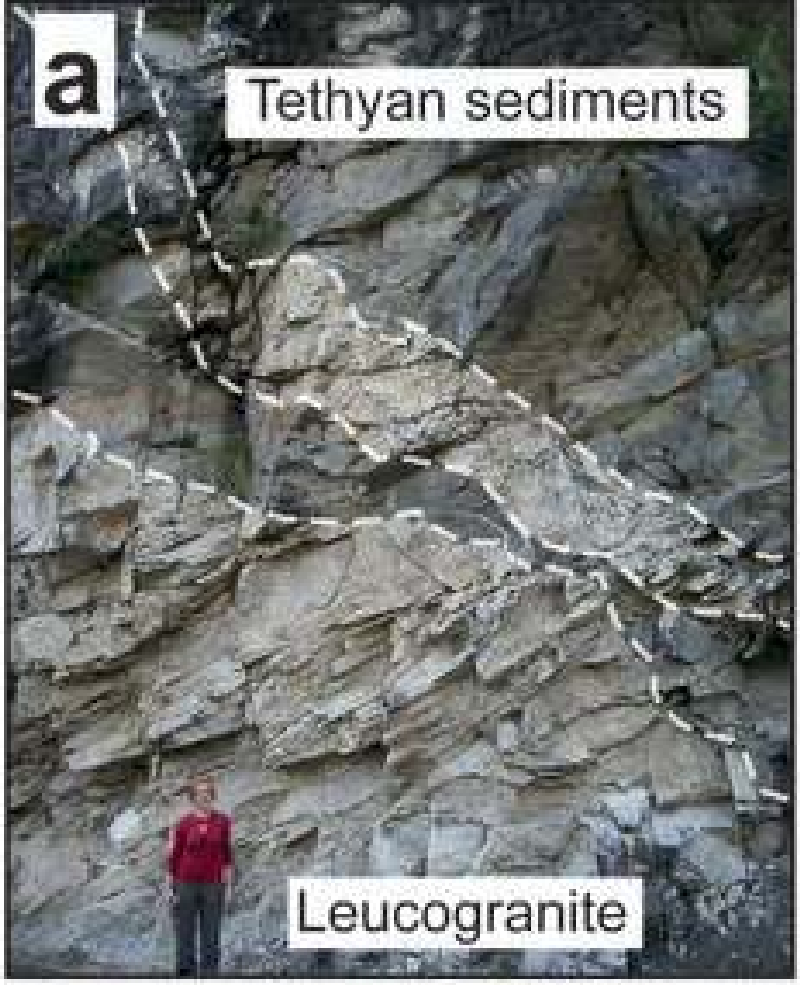
a
Tethyan sediments
Leucogranite

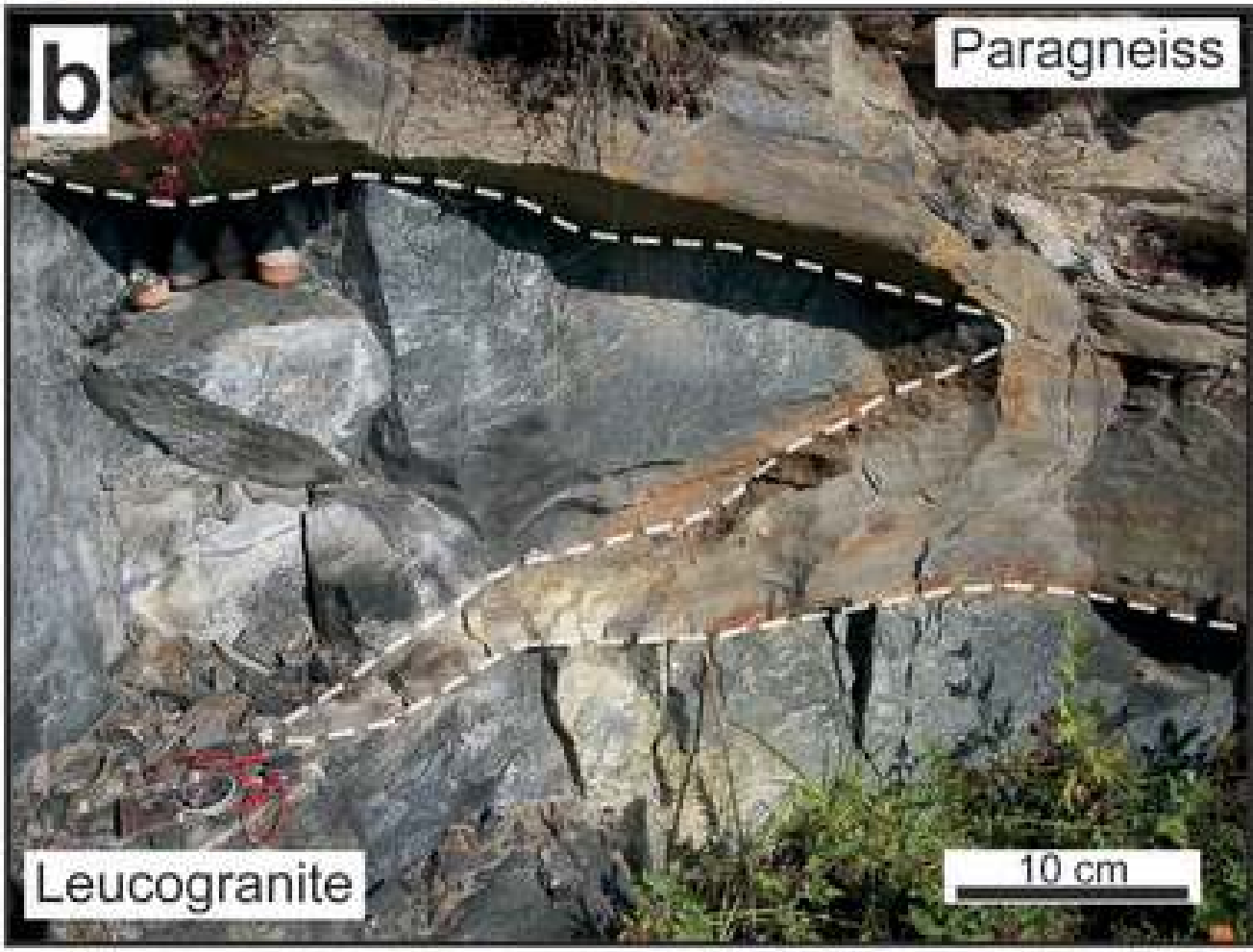
b
Paragneiss
Leucogranite
10 cm

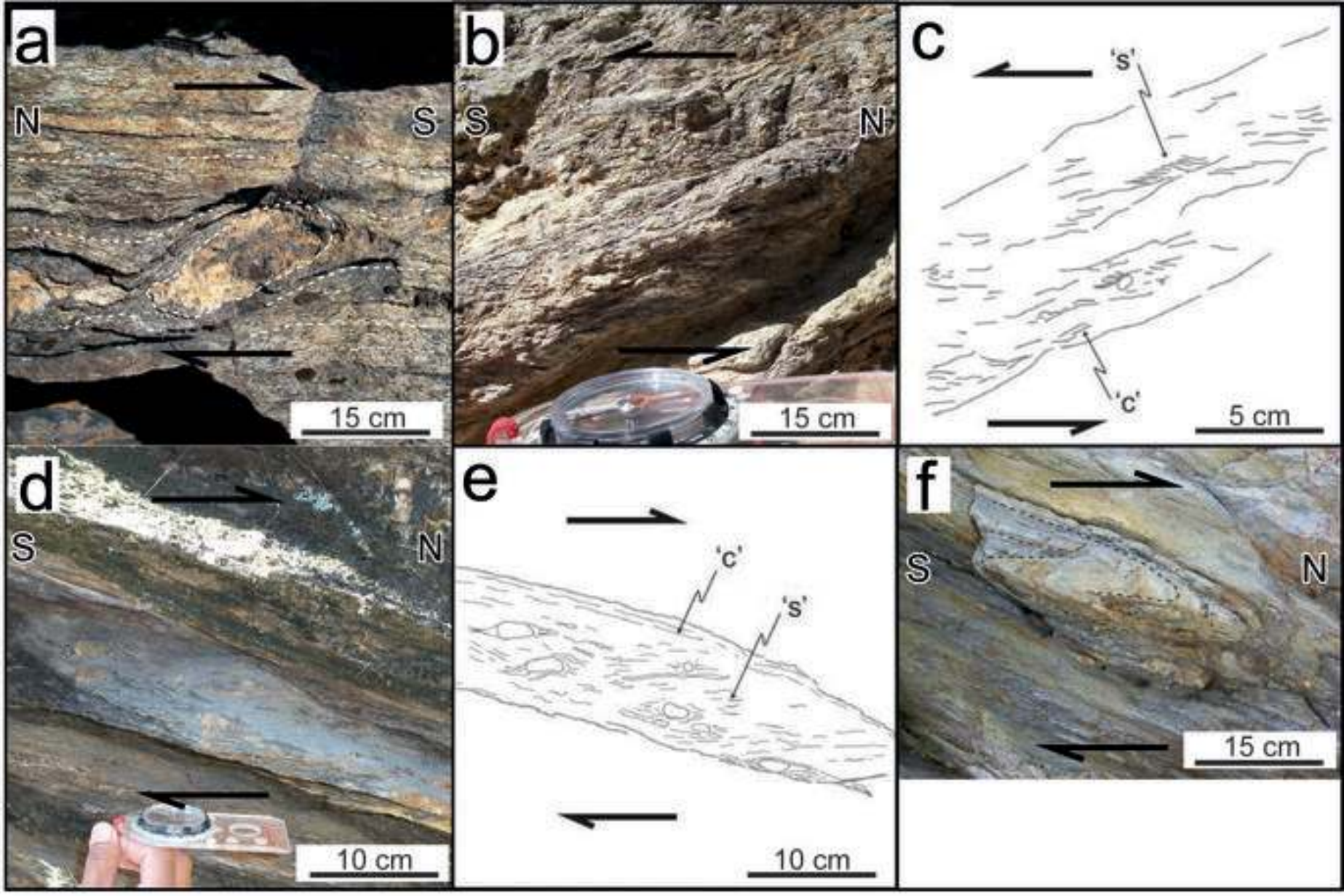
a
N
S
15 cm
b
S
N
15 cm
c
's'
'c'
5 cm
d
S
N
10 cm
e
'c'
's'
10 cm
f
S
N
15 cm

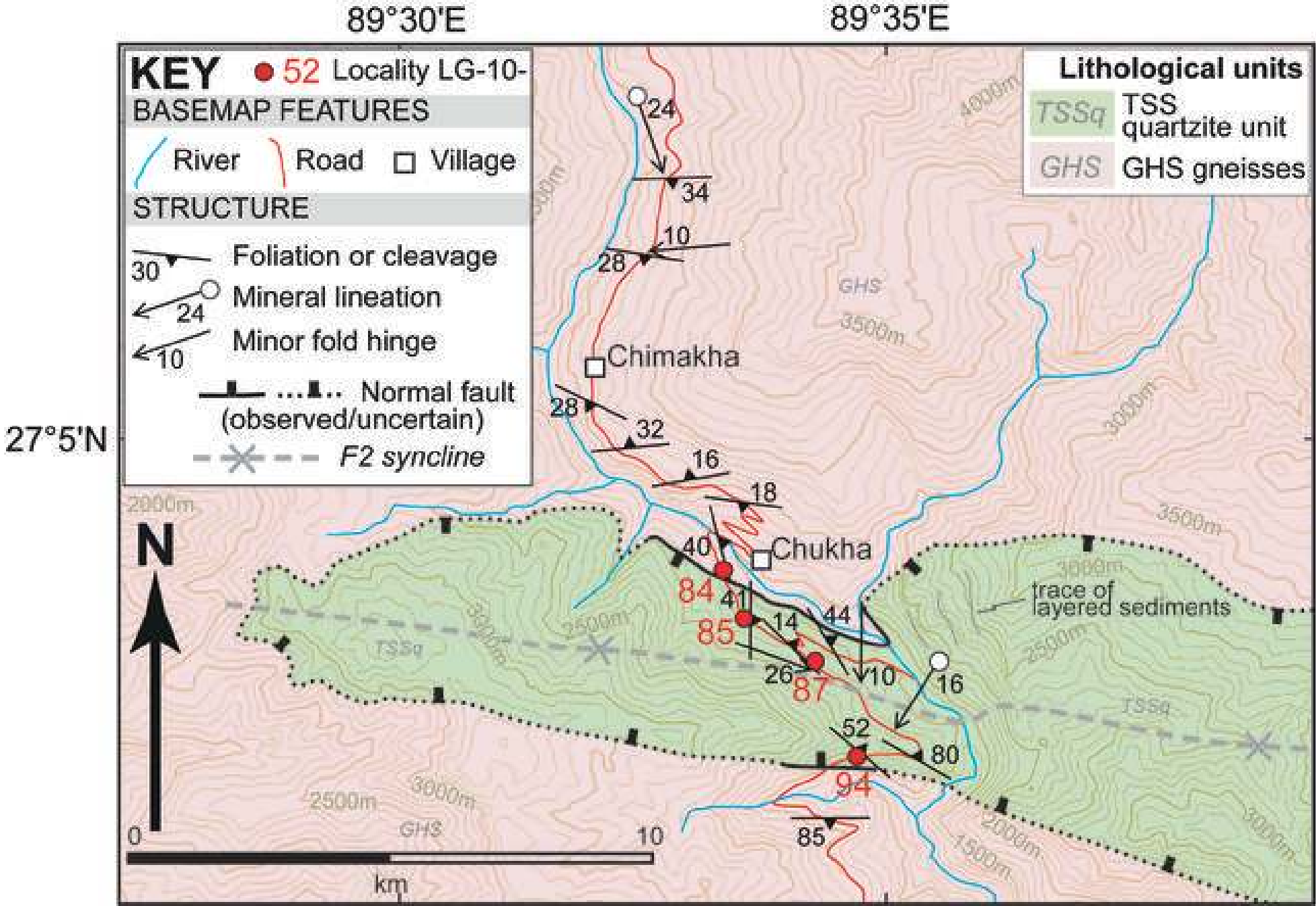
89°30'E
89°35'E
27°5'N
KEY
52 Locality LG-10-
BASEMAP FEATURES
River
Road
Village
STRUCTURE
Foliation or cleavage
Mineral lineation
Minor fold hinge
Normal fault (observed/uncertain)
F2 syncline
Lithological units
TSSq TSS quartzite unit
GHS GHS gneisses
Chimakha
Chukha
trace of layered sediments
N
0
10
km
2000m
2500m
3000m
3500m
4000m
1500m
TSSq
GHS

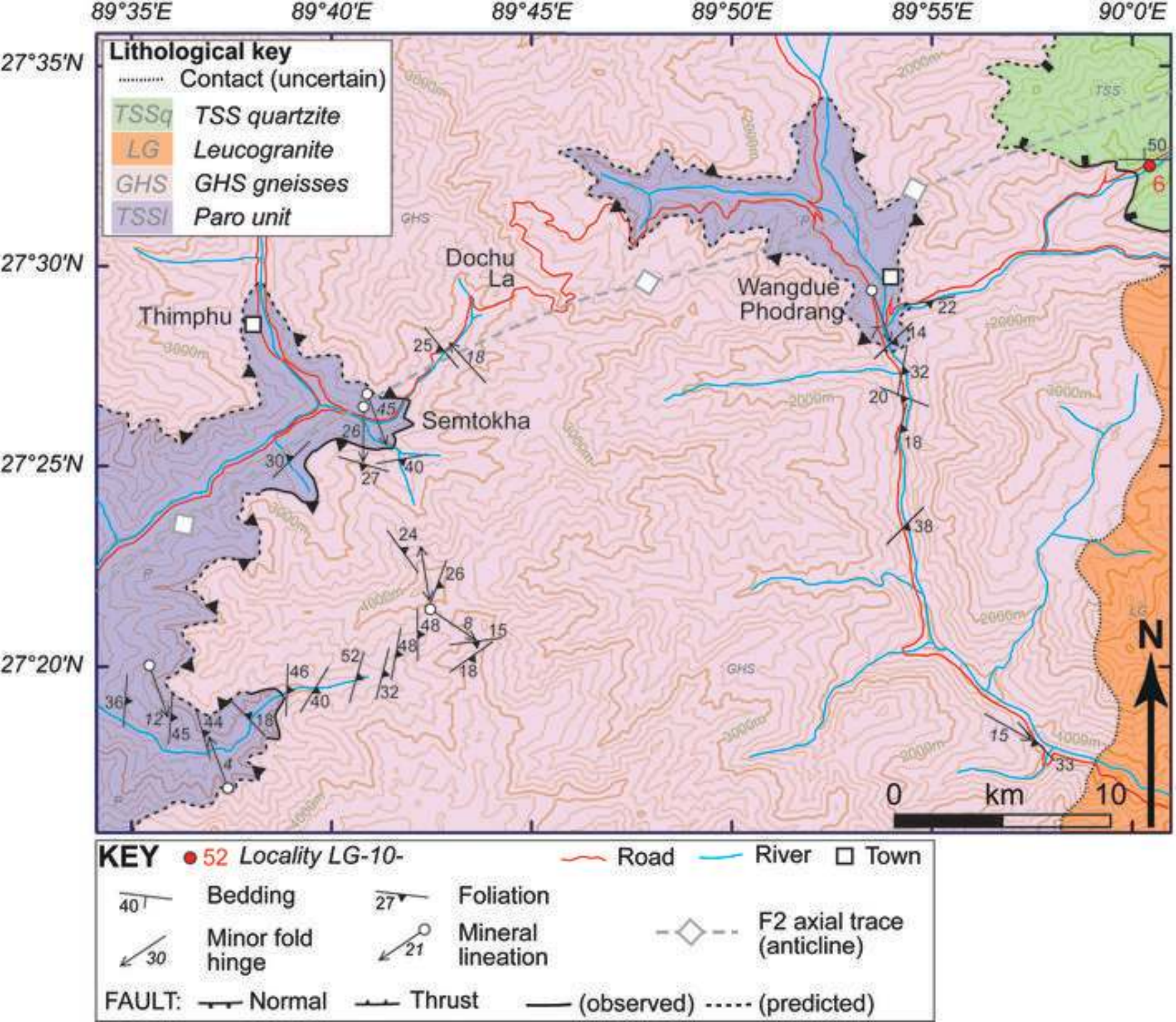
89°35'E
89°40'E
89°45'E
89°50'E
89°55'E
90°0'E
27°35'N
27°30'N
27°25'N
27°20'N
Lithological key
Contact (uncertain)
TSSq TSS quartzite
LG Leucogranite
GHS GHS gneisses
TSSl Paro unit
Thimphu
Dochu La
Semtokha
Wangdue Phodrang
0 km 10
N
KEY
52 Locality LG-10-
Road
River
Town
Bedding
Foliation
Minor fold hinge
Mineral lineation
F2 axial trace (anticline)
FAULT: Normal Thrust (observed) (predicted)

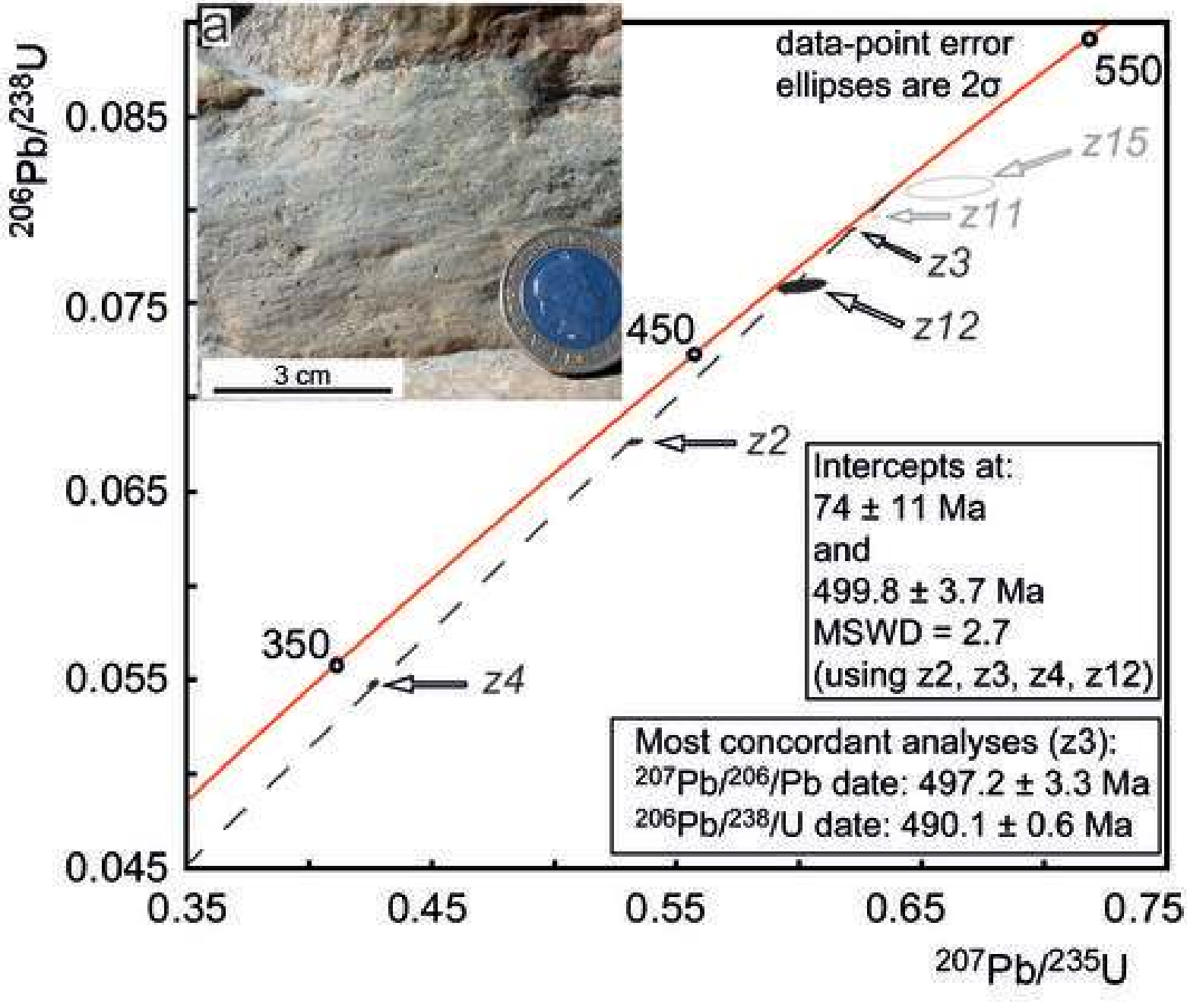
a
3 cm
data-point error
ellipses are 2σ
550
450
350
z15
z11
z3
z12
z2
z4
Intercepts at:
74 ± 11 Ma
and
499.8 ± 3.7 Ma
MSWD = 2.7
(using z2, z3, z4, z12)
Most concordant analyses (z3):
207Pb/206/Pb date: 497.2 ± 3.3 Ma
206Pb/238/U date: 490.1 ± 0.6 Ma
0.085
0.075
0.065
0.055
0.045
0.35
0.45
0.55
0.65
0.75
206Pb/238U
207Pb/235U

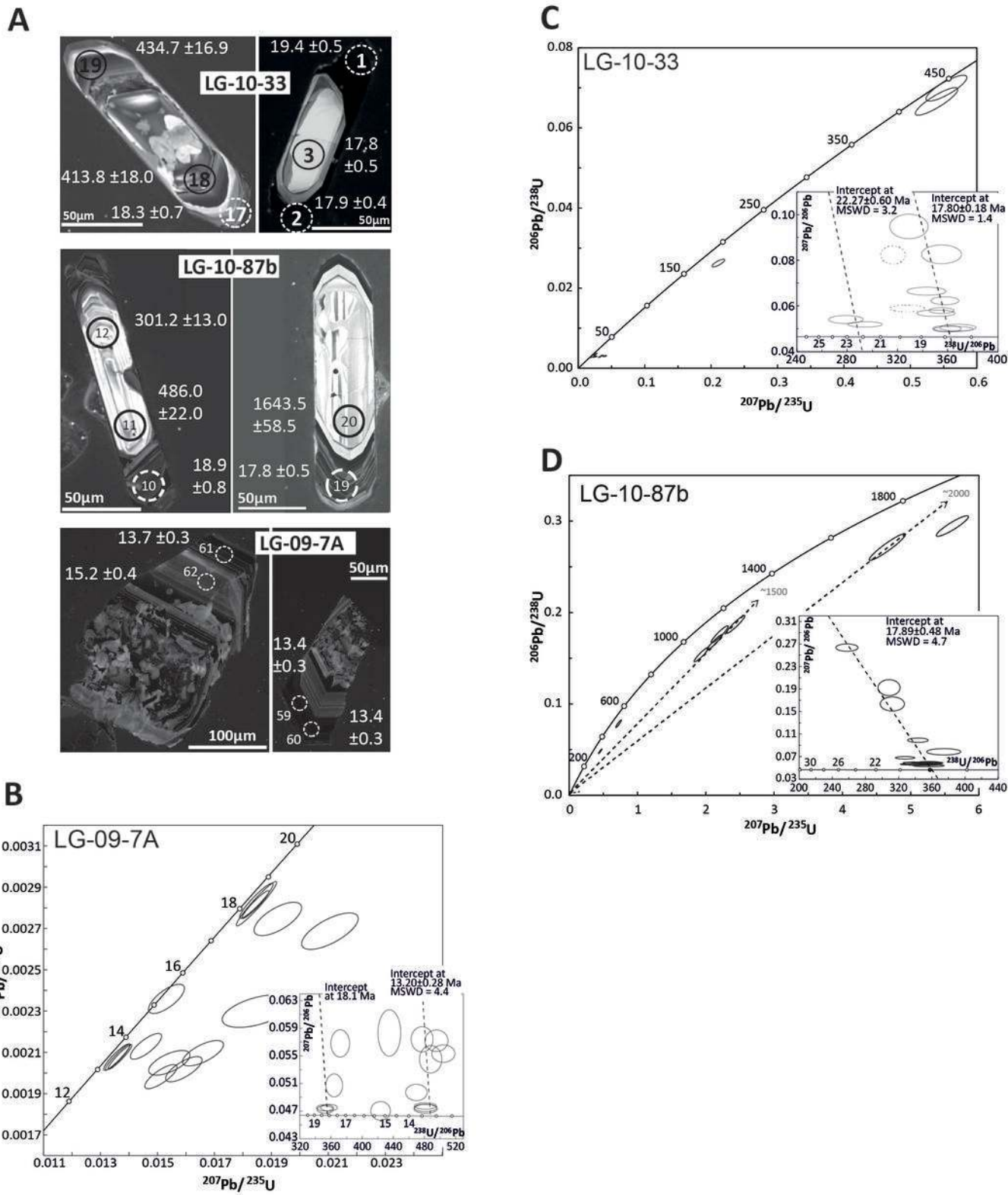
A
LG-10-33
434.7 ±16.9
19.4 ±0.5
413.8 ±18.0
18.3 ±0.7
17,8 ±0.5
17.9 ±0.4
50µm
LG-10-87b
301.2 ±13.0
486.0 ±22.0
1643.5 ±58.5
18.9 ±0.8
17.8 ±0.5
LG-09-7A
13.7 ±0.3
15.2 ±0.4
13.4 ±0.3
13.4 ±0.3
100µm
B
LG-09-7A
Intercept at 18.1 Ma
Intercept at 13.20±0.28 Ma MSWD = 4.4
206Pb/238U
207Pb/235U
C
LG-10-33
Intercept at 22.27±0.60 Ma MSWD = 3.2
Intercept at 17.80±0.18 Ma MSWD = 1.4
206Pb/238U
207Pb/235U
D
LG-10-87b
Intercept at 17.89±0.48 Ma MSWD = 4.7
206Pb/238U
207Pb/235U

Table 1 Summary criteria for determining lithotectonic affinity in Bhutan

Unit	Metamorphic grade	Partial melting	Mineralogy	Deformation	Granitoids	Rock types
TSS	Low (lower greenschist facies, reaching lower amphibolite facies near base)	No evidence	Predominately detrital; Ms widespread; Bt common towards lower levels; Grt in lower micaschists, ± rare St	Tight folding of primary layers, + axial-planar cleavage; foliated in lower portions; later upright folds and crenulations; bedding discernible in some rock types	Miocene granitoid dykes, sills (lower levels, mainly discordant)	Fine to medium grained psammite–quartzite, shale and phyllite (some graphitic or sulphidic); limestone (some fossiliferous, commonly recrystallized); coarser micaschist generally at lowest structural levels
GHS	High (upper amphibolite facies)	Evidence widespread in fertile rocks, but fairly low proportion of migmatites	Grt, Bt common; Ms absent at high grades, but common as retrograde phase; Sil quite common (mainly as fibrolite, + reddish-brown Bt); St rare (inclusions in Grt); Ky rare, but widespread in lower GHS	Pervasive foliation, high strain common, primary bedding unrecognizable	~35-18 Ma, ~500 Ma, ~830 Ma	Leucogneiss, leucogranite ± Tur, uncommon mafic amphibolite; paragneiss, semi-pelitic schist, quartzite, migmatite; less pelitic schist, calc-silicate rock, marble
Paro	Middle amphibolite facies	No evidence; segregations invariably Qtz	Prograde Ms, Bt common; Grt, Hbl locally common in appropriate bulk compositions; St, Ky only at a few localities; AlSilicate polymorphs generally absent	Pervasive foliation, widespread folding; very rare evidence of bedding (vague cross-stratification, etc.)	uncommon, foliated granitic rocks	Psammite, pelite, semi-pelite (incl. rusty sulphidic schist); carbonate rocks, calc-silicate rocks; uncommon deformed micaceous granitoids

Table 2 Summary criteria for identifying major shear zones in Bhutan

Shear zone	Strain	Fabrics	Hanging wall	Footwall	Shear sense	Other features
STD	Narrow zone of highest ductile shear strain within ~200-300m zone with increased flattening and simple shear strain	More intense shear fabrics in narrow zone; late or post-kinematic Bt or Ms + annealed microfabrics in hanging wall	Finer-grained, low grade quartzite; some Bt-Ms phyllite/schist ± Grt; carbonate rock may overlie these (TSS)	Upper amphibolite facies gneiss or schist, locally migmatitic; retrograde Ms common (GHS)	N-directed in narrow zone of highest strain at lithological transition; C-S fabrics, shear bands	Leucogranite sills, most deformed + concordant in footwall; some mask contact; discordant dykes + sills in hanging wall
MCT	High to very high ductile strain predominant and conspicuous in both footwall and hanging wall	Strong, ductile, often mylonitic/ultramylonitic fabrics; C-S fabrics; high grade (Grt + Sil ± Ky); L-S tectonites common	Upper amphibolite facies gneiss, higher pressure assemblages than footwall, high-strain, rare leucosomes (GHS)	Thin micaschist ± Chl; quartzite (mainly thick); flaggy, greenschist mylonite; some shale, carbonate rock (LHS)	S-directed, strong: C-S fabrics, other asymmetric fabrics, porphyroblast systems	Thin section of scaly micaschist (Jaishidanda unit) along shear zone

Table 3. U-Pb ID-TIMS data for the ashbed sample LG-09-21

Compositional Parameters							Radiogenic Isotope Ratios								Isotopic Ages					
Sample	Th/U	$^{206}Pb^{*}$ x10^{-13} mol	mol % $^{206}Pb^{*}$	Pb*/Pbc	Pbc (pg)	$^{206}Pb/^{204}Pb$	$^{208}Pb/^{206}Pb$	$^{207}Pb/^{206}Pb$	% err	$^{207}Pb/^{235}U$	% err	$^{206}Pb/^{238}U$	% err	corr. coef.	$^{207}Pb/^{206}Pb$	±	$^{207}Pb/^{235}U$	±	$^{206}Pb/^{238}U$	±
(a)	(b)	(c)	(c)	(c)	(c)	(d)	(e)	(e)	(f)	(e)	(f)	(e)	(f)		(g)	(f)	(g)	(f)	(g)	(f)
LG-09-21																				
z2	0.71	0.48	98.1%	17.0	0.8	994	0.23	0.05712	0.36	0.5334	0.43	0.06773	0.12	0.71	495.7	7.9	434.1	1.5	422.5	0.50
z3	0.72	1.46	99.4%	56.2	0.7	3242	0.23	0.05716	0.15	0.6224	0.24	0.07898	0.12	0.84	497.2	3.3	491.3	0.9	490.1	0.57
z4	0.59	0.65	99.4%	56.4	0.3	3341	0.19	0.05644	0.16	0.4266	0.25	0.05483	0.13	0.81	469.1	3.5	360.8	0.7	344.2	0.42
z11	0.27	3.50	99.7%	111.7	0.7	7220	0.09	0.05757	0.10	0.6324	0.18	0.07966	0.09	0.95	513.1	2.2	497.6	0.7	494.2	0.42
z8	0.58	1.61	99.4%	54.2	0.8	3052	0.18	0.13489	0.12	6.4592	0.24	0.34730	0.17	0.88	2163	2.1	2040	2.1	1922	2.81
z12	0.41	1.52	84.6%	1.6	23.2	116	0.13	0.05739	1.28	0.6018	1.39	0.07605	0.39	0.41	506.1	28.2	478.4	5.3	472.6	1.76
z15	0.45	2.65	84.5%	1.6	40.5	116	0.14	0.05912	2.01	0.6623	2.16	0.08125	0.50	0.39	571.1	43.8	516.0	8.7	503.6	2.45

locality coordinates: 27.28155°E, 90.62450°N

(a) z1, z2 etc. indicate fractions composed of single zircon grains or fragments; all fractions annealed and chemically abraded after Mattinson (2005).

(b) Model Th/U ratio calculated from radiogenic $^{208}Pb/^{206}Pb$ ratio and $^{207}Pb/^{235}U$ age.

(c) Pb* and Pbc represent radiogenic and common Pb, respectively; mol % $^{206}Pb^{*}$ with respect to radiogenic, blank and initial common Pb.

(d) Measured ratio corrected for spike and fractionation only.

(e) Corrected for fractionation, spike, and common Pb; up to 2 pg of common Pb was assumed to be procedural blank: $^{206}Pb/^{204}Pb = 18.60 \pm 0.80\%$; 207Pb/204Pb = 15.69 ± 0.32%; 208Pb/204Pb = 38.51 ± 0.74% (all uncertainties 1-sigma). Excess over blank was assigned to initial common Pb.

(f) Errors are 2-sigma, propagated using the algorithms of Schmitz and Schoene (2007).

(g) Calculations are based on decay constants of Jaffey et al. (1971). $^{206}Pb/^{238}U$ and $^{207}Pb/^{206}Pb$ ages corrected for initial disequilibrium in $^{230}Th/^{238}U$ using Th/U [magma] = 3 using the algorithms of Schärer (1984).

(h) dates in bold are those included in weighted mean calculations. See text for discussion.

Sample number	Form	Host unit(s)	Cross-cuts structures?	Petrological type	Deformed?	Mineralogy[a]					Zircon ages, Ma		
						biotite	garnet	muscovite	tourmaline	chlorite	Rim $^{206}Pb/^{238}U$ age	Additional $^{206}Pb/^{238}U$ age	Core $^{206}Pb/^{238}U$ age
LG-09-7A	dyke	GHS	YES	pegmatite	no			■			**13.20 ± 0.28**	c. 18.1	
LG-10-33	dyke	TSS	YES	tourmaline	no			■	■		**17.80 ± 0.18**	22.27 ± 0.60	
LG-10-87B	dyke	TSS	YES	tourmaline	no	■			■	■	**17.89 ± 0.48**		>1500

[a] all granites contain quartz and feldspar

Grain	Analysis number	raster, r or spot, s	Pb, ppm	U, ppm	Uncorrected isotopic ratios							Uncorrected ages					Common lead corrected isotopic ratios		Common lead corrected ages	
					$^{207}Pb/^{206}Pb$	1σ, %	$^{207}Pb/^{235}U$	1σ, %	$^{206}Pb/^{238}U$	1σ, %	Rho	$^{206}Pb/^{238}U$	2σ, abs	$^{207}Pb/^{235}U$	2σ, abs	*f206,* %	$^{206}Pb^*/^{238}U$	1σ, %	$^{206}Pb^*/^{238}U$	2σ, Ma
LG-09-7A ***(27.47178°N, 90.47928°E, Pegmatite dyke within GHS)***																				
5	1	s	10	151	0.0501	1.6	0.0186	2.1	0.00269	1.3	0.634	17.3	0.5	18.7	0.8	0.005	0.00268	1.3	17.2	0.5
5	2	s	3	27	0.0514	2.7	0.0163	3.0	0.00230	1.4	0.456	14.8	0.4	16.4	1.0	0.006	0.00228	1.4	14.7	0.4
5	3	s	10	167	0.0481	1.7	0.0136	2.1	0.00205	1.2	0.573	13.2	0.3	13.7	0.6	0.002	0.00204	1.2	13.2	0.3
6	4	s	13	328	0.0505	1.3	0.0140	1.8	0.00202	1.2	0.694	13.0	0.3	14.2	0.5	0.005	0.00201	1.2	12.9	0.3
6	5	s	17	583	0.0488	1.1	0.0133	1.6	0.00198	1.2	0.752	12.8	0.3	13.5	0.4	0.003	0.00198	1.2	12.7	0.3
7	6	s	10	242	0.0506	1.5	0.0146	1.9	0.00210	1.2	0.630	13.5	0.3	14.7	0.6	0.005	0.00208	1.2	13.4	0.3
1	55	s	21	8371	0.0507	1.3	0.0192	1.8	0.00275	1.2	0.668	17.7	0.4	19.3	0.7	0.006	0.00273	1.2	17.6	0.4
2	56	s	38	14723	0.0475	0.4	0.0186	1.3	0.00284	1.3	0.957	18.3	0.5	18.7	0.5	0.001	0.00283	1.3	18.2	0.5
2	57	s	39	15749	0.0475	0.4	0.0183	1.3	0.00280	1.2	0.951	18.0	0.4	18.4	0.5	0.001	0.00279	1.2	18.0	0.4
2	58	s	32	12714	0.0472	0.5	0.0185	1.3	0.00284	1.2	0.937	18.3	0.4	18.6	0.5	0.001	0.00283	1.2	18.2	0.4
3	59	s	32	16932	0.0475	0.5	0.0136	1.3	0.00208	1.2	0.937	13.4	0.3	13.7	0.4	0.002	0.00207	1.2	13.4	0.3
3	60	s	38	20096	0.0477	0.4	0.0137	1.3	0.00208	1.2	0.948	13.4	0.3	13.8	0.3	0.002	0.00207	1.2	13.4	0.3
4	61	s	22	11270	0.0497	1.0	0.0146	1.5	0.00213	1.2	0.783	13.7	0.3	14.7	0.5	0.004	0.00212	1.2	13.7	0.3
4	62	s	11	4974	0.0470	1.2	0.0153	1.7	0.00236	1.2	0.718	15.2	0.4	15.4	0.5	0.001	0.00236	1.2	15.2	0.4
8	63	s	26	13739	0.0474	0.5	0.0136	1.4	0.00208	1.3	0.918	13.4	0.3	13.7	0.4	0.001	0.00207	1.3	13.4	0.3
LG-10-33 ***(27.71674°N, 90.28676°E Granite dyke cutting through Tethyan sediments)***																				
1	1	s	16	5076	0.0823	2.0	0.0359	2.4	0.00316	1.2	0.526	20.3	0.5	35.8	1.7	0.045	0.00302	1.2	19.4	0.5
1	2	s	56	19868	0.0579	0.9	0.0225	1.4	0.00282	1.2	0.800	18.1	0.4	22.6	0.6	0.015	0.00278	1.2	17.9	0.4
1	3	s	33	11921	0.0500	1.1	0.0192	1.7	0.00278	1.3	0.749	17.9	0.5	19.3	0.7	0.005	0.00277	1.3	17.8	0.5
2	4	s	56	20021	0.0622	1.2	0.0240	1.7	0.00280	1.3	0.742	18.0	0.5	24.1	0.8	0.020	0.00274	1.3	17.6	0.5
2	5	s	57	3846	0.0826	2.0	0.0321	2.7	0.00282	1.8	0.667	18.1	0.7	32.1	1.7	0.046	0.00269	1.8	17.3	0.6
2	5.1	s	97	35125	0.0505	1.2	0.0189	2.0	0.00272	1.6	0.810	17.5	0.6	19.0	0.7	0.005	0.00270	1.6	17.4	0.6
3	6	s	23	1471	0.0519	0.9	0.0243	2.1	0.00340	1.9	0.901	21.9	0.8	24.4	1.0	0.007	0.00338	1.9	21.7	0.8
3	7	s	20	1216	0.0540	1.3	0.0267	2.4	0.00358	2.0	0.841	23.1	0.9	26.8	1.3	0.010	0.00355	2.0	22.8	0.9
7	10	s	15	662	0.0568	1.1	0.0223	2.1	0.00285	1.8	0.861	18.4	0.7	22.4	0.9	0.013	0.00281	1.8	18.1	0.7
9	13	s	28	1532	0.0499	0.8	0.0189	2.0	0.00274	1.8	0.911	17.7	0.6	19.0	0.7	0.005	0.00273	1.8	17.6	0.6
4	17	s	117	8520	0.0665	1.1	0.0267	2.2	0.00291	1.8	0.854	18.8	0.7	26.8	1.1	0.025	0.00284	1.9	18.3	0.7
4	18	s	256	8129	0.0587	1.2	0.5393	2.4	0.06660	2.1	0.870	415.7	17.0	438.0	17.1	0.005	0.06630	2.1	413.8	18.0
4	19	s	368	357	0.0575	1.3	0.5541	2.3	0.06992	1.9	0.829	435.7	15.8	447.7	16.3	0.002	0.06976	1.9	434.7	16.9
6	20	s	114	2191	0.0948	2.3	0.0397	3.0	0.00304	1.9	0.632	19.6	0.7	39.6	2.3	0.061	0.00285	1.9	18.4	0.7
6	21	s	41	623	0.0589	1.0	0.0248	2.0	0.00305	1.8	0.866	19.6	0.7	24.8	1.0	0.016	0.00300	1.8	19.3	0.7
LG-10-87B ***(27.04453°N, 89.57191°E Granite dyke in Metasediments at Chukha)***																				
1	1	s	276	3923	0.0786	0.7	1.8150	2.2	0.16741	2.1	0.943	997.8	38.1	1050.9	28.3	0.007	0.16616	2.1	990.9	44.1
1	2	s	138	988	0.0777	0.9	1.6498	2.3	0.15397	2.1	0.920	923.2	36.2	989.5	28.6	0.009	0.15251	2.1	915.0	41.4
2	3	s	41	493	0.0806	0.9	2.0784	2.3	0.18707	2.1	0.929	1105.5	43.3	1141.7	31.1	0.005	0.18614	2.1	1100.4	51.2
2	4	s	98	846	0.0773	1.0	1.8782	2.4	0.17619	2.2	0.913	1046.1	41.7	1073.4	31.0	0.004	0.17552	2.2	1042.5	48.9
3	5	s	12	51	0.0460	1.7	0.0178	2.7	0.00281	2.2	0.793	18.1	0.8	17.9	1.0	0.000	0.00281	2.2	18.1	0.8
3	6	s	11	60	0.2247	1.2	0.1202	2.4	0.00388	2.1	0.873	25.0	1.1	115.3	5.3	0.225	0.00301	2.1	19.4	0.8
4	7	s	2	13	0.0670	3.4	0.0247	4.1	0.00267	2.2	0.550	17.2	0.8	24.7	2.0	0.026	0.00260	2.2	16.7	0.8
4	8	s	7	50	0.0482	1.7	0.0193	2.8	0.00290	2.2	0.783	18.7	0.8	19.4	1.1	0.002	0.00289	2.2	18.6	0.8
4	9	s	81	264	0.1060	0.9	3.9709	2.4	0.27172	2.2	0.924	1549.5	60.1	1628.3	37.7	0.011	0.26860	2.2	1533.7	75.5
5	10	s	11	114	0.0480	1.2	0.0195	2.5	0.00294	2.1	0.869	19.0	0.8	19.6	1.0	0.002	0.00294	2.1	18.9	0.8
5	11	s	65	1388	0.0570	0.9	0.6156	2.4	0.07832	2.2	0.919	486.1	20.4	487.1	18.2	0.000	0.07831	2.2	486.0	22.0
5	12	s	54	950	0.0582	0.9	0.3865	2.3	0.04818	2.1	0.921	303.3	12.5	331.8	12.9	0.007	0.04783	2.1	301.2	13.0
9	13	s	13	11	0.0466	1.4	0.0180	2.0	0.00280	1.5	0.733	18.0	0.5	18.1	0.7	0.000	0.00280	1.5	18.0	0.5
11	14	s	1	6	0.1359	3.8	0.0600	4.2	0.00320	1.9	0.453	20.6	0.8	59.2	4.8	0.113	0.00284	1.9	18.3	0.7
13	16	s	13	493	0.0489	1.4	0.0200	2.0	0.00297	1.4	0.706	19.1	0.5	20.1	0.8	0.003	0.00296	1.4	19.0	0.5
13	17	s	17	402	0.0487	1.3	0.0193	1.9	0.00287	1.4	0.754	18.5	0.5	19.4	0.7	0.003	0.00286	1.4	18.4	0.5
13	18	s	9	162	0.0564	1.6	0.0237	2.2	0.00305	1.5	0.669	19.6	0.6	23.8	1.0	0.013	0.00301	1.5	19.4	0.6
14	19	s	19	431	0.0490	1.3	0.0187	1.9	0.00277	1.5	0.759	17.9	0.5	18.9	0.7	0.003	0.00277	1.5	17.8	0.5
14	20	s	199	1006	0.1148	0.8	4.6651	1.8	0.29468	1.6	0.880	1664.9	45.7	1761.0	29.3	0.015	0.29040	1.6	1643.5	58.5
15	21	s	9	34	0.0482	1.8	0.0185	2.4	0.00278	1.5	0.632	17.9	0.5	18.6	0.9	0.002	0.00278	1.5	17.9	0.5
15	22.2	s	11	58	0.0823	1.9	0.0331	2.4	0.00291	1.5	0.619	18.8	0.6	33.1	1.6	0.045	0.00278	1.5	17.9	0.5
16	23	s	18	140	0.0498	1.3	0.0193	1.9	0.00281	1.4	0.746	18.1	0.5	19.4	0.7	0.004	0.00279	1.4	18.0	0.5
17	24	s	2	3	0.1600	3.6	0.0715	4.0	0.00324	1.8	0.438	20.9	0.7	70.1	5.4	0.144	0.00278	1.8	17.9	0.6